A hydrodynamical reconstruction of the last major merger of the Milky Way

by

Julien Marabotto
URN: 6598122

For the degree of Master of Physics in

Physics with Nuclear Astrophysics

Submitted on 11th January, 2023

This dissertation and the work to which it refers are the results of my own efforts. Any ideas, data, images or text resulting from the work of others (whether published or unpublished) are fully identified as such within the work and attributed to their originator in the text, bibliography or in footnotes. This dissertation has not been submitted in whole or in part for any other academic degree or professional qualification. I agree that the University has the right to submit my work to the plagiarism detection service TurnitinUK for originality checks. I own the copyrights.

Abstract

The discovery that the Galactic stellar halo is not only formed by the oldest stars in the Milky Way, but also made up of stars that have ages and abundances typical of disc populations, has led to the identification of a distinct stellar population within the Galaxy. This has been associated to the debris remaining from the accretion of a massive dwarf galaxy: Gaia-Sausage-Enceladus (GSE). In recent years, the question regarding whether this major merger was indeed a single accretion event has gained in popularity, with claims that a second dwarf galaxy, Sequoia, must have merged with the Milky Way to account for a retrograde population in the Galactic halo. By running a series of N-body, hydrodynamical simulations between the Milky Way progenitor and a massive GSE-like satellite, we seek to verify the self-consistency of a single GSE-merger event by attempting to understand the impact of gas on the kinematic properties of the major merger, as well as its imprint in the present day kinematic-space of the Milky Way stellar halo. From our list of models, we find that a gas-rich, GSE-progenitor on a retrograde orbit with $M_{gas} = 8 \times 10^9 M_\odot$, $M_{star} = 2.1 \times 10^9 M_\odot$ and $M_{DM} = 4.73 \times 10^{10} M_\odot$ most robustly reproduces the significant properties observed in the kinematic space of the Galactic halo. More importantly, we show that a model with such properties is sufficient in reproducing merger debris with properties similar to those attributed to Sequoia, which goes to show that the hydrodynamical impact of gas on N-body simulations cannot be neglected when modelling galaxy pair mergers. We highlight the importance of upcoming spectroscopic surveys in further disentangling debris populations and building upon the work we present.

Keywords: Milky Way, Gaia-Sausage-Enceladus, Sequoia, galaxy merger, hydrodynamical

Contents

List of Figures

List of Tables

Abbreviations

Acknowledgements

Chapter 1

Introduction

The Universe is populated by an estimated two trillion galaxies [2], each drifting apart from the other as a result of the expansion of space driven by dark energy. Amongst these, located in the Laniakea Supercluster [3], we find our home – the Milky Way (MW) galaxy. The structure of the Milky Way is complex and continuously evolving, notably due to internal processes (bar, spiral arms instabilities) and gravitational interactions experienced between itself and nearby, orbiting galaxies throughout its past, present and foreseeable future.

A typical galaxy, like the Milky Way, can be defined as a gravitationally bound set of stars, gas and dust whose properties, however, cannot be explained by a combination of baryons and Newton's laws of gravity. This implies that luminous matter alone is insufficient in explaining the complex dynamics of galaxies [4]; a galaxy must therefore rely on some form of electromagnetically non-interactive "dark" matter to remain gravitationally bound as a single entity. Its gravitational influence was found to be imprinted in the rotation curves of a selection of type-C spiral galaxies [5], demonstrating that galaxies are embedded in dark matter (DM) halos extending to large radii from their center. Although the nature of DM is still unknown, its existence is widely accepted and predicted by the cosmological models that lay the foundations of modern cosmology, namely a dark energy and cold dark matter dominated cosmological model of the Universe (ΛCDM).

The ΛCDM model describes the collapse of infinitesimal density perturbations in the substructure of the early Universe, observable in the Cosmic Microwave Background (CMB) [6], as the origin of galaxy formation; DM halos resulting from the collapse of these density anisotropies gravitationally interact and grow through hierarchical clustering, leading to the accretion of gas through large-scale filaments in the cosmic web and, subsequently, to the formation of galaxies [7, 8, 9, 10]. In addition to being permanently 'fed' by the inflow of gas, galaxies also grow more massive through continuous mergers with smaller nearby systems [11, 8]. The spatial distributions of matter components (DM, gas and stellar) for the Local Group, nicely illustrated by Scannapieco et al. (2015) [12] which we show in Fig. 1.1, reveal the large amounts of

substructure in the Cosmic web.

Following the release of the Sloan Digital Sky Survey (SDSS)[13] and the subsequent discovery of large amounts of sub-structure in the stellar halo of the Milky Way, including merger remnants in the form of shells, stream, filaments and tidal tails [14, 15, 16], the Milky Way has been found to be the epitome of ΛCDM cosmology. Our understanding of the dynamical structure of the Galactic halo is currently undergoing a major paradigm shift, thanks to superb data from the Gaia (ESA) satellite. The rise of modern spectroscopic surveys such as the Apache Point Observatory Galactic Evolution Experiment (APOGEE), Galah, the Large Sky Area Multi-Object Fiber Spectroscopic Telecope (LAMOST) and the upcoming ones (4MOST, MOONS, WEAVE) reflects the intention of the astrophysicist community to uncover the origin of the Galaxy and its halo in the coming years. These complementary missions provide unprecedented instrumentation which, combined, hold the power to map out and analyse motions, luminosities, temperatures and chemical compositions of millions of stars across our galaxy [17, 18]. In turn, the gathered data will greatly contribute to unravelling the mysteries of the MW galaxy formation, evolution and present-day structure of its different components (disk, bulge and halo).

1.1 The stellar halo of the Milky Way

1.1.1 Origin and Structure

The Galactic halo contains <1% of the stellar mass of the Milky Way [19], with recent analysis calculating the total stellar mass of the halo as $M_{\star,\text{tot}} = 1.3^{+0.3}_{-0.2} \times 10^9 M_{\odot}$ using a sample of APOGEE red giant stars [20]. Of this stellar mass, approximately $0.9^{+0.2}_{-0.1} \times 10^9 M_{\odot}$ is estimated to belong to accreted populations. The stellar halo of the Milky Way is the home of the most metal-poor stars of our galaxy, which have lifetimes comparable to the current age of the Universe [21]. It therefore holds one of the most powerful archaeological tools in partially uncovering the appearance of the Milky Way in the past [22, 23], as the chemical elements imprinted in the atmospheres of halo stars reflect the physical conditions of the interstellar medium in which they were born [23]. Thus, we can trace their birth site from their chemical abundance and orbital motions.

While there is mounting evidence that the inner regions of the Milky Way may - for the very large majority - be made of stars formed in the Galaxy itself over time, it is in the stellar halo that we need to look to find traces of past and ongoing satellite accretion events. Numerical simulations indeed suggest that the stellar halos of disk galaxies like the Milky Way may contain hundreds of stellar streams, which are relics of mergers with other galactic systems with masses comparable to or significantly smaller than our own Galaxy at the time of their accretion [24, 25, 26]. The origin of

the stellar halo of the Milky Way remains to this day a major topic of conversation in Galactic astronomy; whether the Galactic halo was predominantly formed "in-situ" [1] [22] or whether most its stars were primarily accreted during merger events involving dwarf satellite galaxies [27, 28, 29, 30] is yet to be answered with certainty.

Although the observed substructure of the Galactic stellar halo is consistent with that of a predominantly accreted stellar halo predicted by cosmological simulations [30], the reality may in fact comprise a combination of both phenomena, with further research suggesting that the halo of the Milky Way contains both stellar populations that formed in-situ as well as others resulting from past accretion events [24, 21, 31]. This may be explained by a division of the Galactic halo into an inner- and outer- component [32, 33]; the inner- halo originating from in-situ star formation and accretion processes consistent with ΛCDM cosmology, while the outer-halo would host the remnants of accreted satellite galaxies [31]. This idea has however been contested due to the lack of evidence from SDSS/Sloan Extension for Galactic Understanding and Exploration (SEGUE) in favour of a dual Galactic halo over a single, sub-structure-rich halo [34].

The different properties of the inner- and outer- Galactic halo are representative of its chemical evolution and merger history. Due to their earlier time of accretion, inner-halo stars should have different chemistry [29, 35] than outer- halo stars, both thanks to their enrichment in α-elements produced during type II supernovae (SNeII) [36] or to the high metallicity composition of relatively massive ($10^8 - 10^{10} M_\odot$) accreted galaxies [35]. This is notably illustrated by an identifiable divide between the metallicity density functions (MDF) and the orbital motions of the outer- and inner stellar halo [32, 37].

Broadly speaking, the accreted component of the stellar halo of the Milky Way is made up of (i) a large number of stellar streams and (ii) a more (nearly) smooth component. Stellar streams are usually linked to dwarf galaxies and globular clusters being disrupted by the tidal forces of the Milky Way. In this case, the orbit of the object can be traced from the tidal stellar stream, which is usually visible in the sky. In the case of streams emerging from the accretion of dwarf galaxies, this suggests a relatively recent perturbation or recent infall. Remnants of galaxies accreted at the very early phases of the Milky Way evolution are in contrast contained in the smooth component of the Galactic halo, along with in-situ formed stellar populations heated up by the mergers at different epochs.

Historically, the accretion scenario dates back to Searle & Zinn (1978) [27], who suggested that the stellar halo was formed from metal-poor satellite galaxies, in which stars undergoing chemical evolution prior to being accreted eventually fell into dynamical equilibrium with the Milky Way. This view was seen as antithetic to the scenario proposed a decade earlier by Eggen et al. (1962) [22], where "the oldest stars were formed out of gas falling toward the galactic center in the radial direction and collapsing from the halo onto the plane" on timescales as short as 10^8 years.

---

[1]In-situ: stars formed within the Milky Way itself; not accreted

While for several decades it has been thought that the stellar halo was the result of the combination of these two processes (see [23, 38] for a review), the most recent works seem to exclude a dominant contribution of the radially "collapsed" component to the inner stellar halo.

However, it has now become evident that the accretion of satellite galaxies is not the only channel to form stellar halos. When satellites are accreted, they damage the disk of the Milky Way, and kinematically "heat" it. Because of this process, Milky Way stars that were confined in the disk before the interaction can be ejected at large heights, contributing to the formation of the halo. As a consequence, not all stars in the halo have an extragalactic origin, but a fraction of them formed in-situ, in the Galactic disc, and were then ejected into the halo. Since we have evidence that the most massive accretions in the Galaxy occurred at early times (i.e. in its first billion years of evolution), this in-situ, kinematically heated component of the stellar halo must be made of stars of the ancient Galactic disk. Until a couple of years ago, this was the scenario traced by numerical simulations (see, for example, [39, 40, 41, 42]). Thanks to Gaia and complementary spectroscopic surveys, we can now demonstrate that these two channels (accretions and in-situ, heated disc) are the main two modes of formation of the inner Galactic halo (inside about 15 kpc from the Galactic center).

1.1.2 Streams in the MW halo

The growth of galaxies through hierarchical clustering described by ΛCDM is expected to result in the disintegration of the accreted satellite, which may be followed by a trail of stripped stars. These elongated structures, formed when a small galaxy or globular cluster is pulled apart by the gravitational forces of a larger galaxy such as the Milky Way, are called tidal streams. Although it is difficult to accurately determine the number of tidal streams that have been discovered in the Milky Way, some estimates claim that the Galaxy contains at least several dozen tidal streams [43, 44]. A number of these were in fact projected by Mateu (2022) into Galactic coordinates [44], which we illustrate in Fig. 1.2 [2] alongside further projections of several real images of stellar streams onto the night sky [3].

Some of the streams have indeed been found in recent years (see, e.g. [45]). The most prominent and famous of them is the Sagittarius stream, a stellar band of stars that wraps around the Galaxy on a polar-like orbit [46, 47]. This stream is made of stars that were once associated to the Sagittarius dwarf galaxy (Sgr) dwarf spheroidal galaxy (the closest Milky Way companion at about 24 kpc from the Sun [48]) and that have been stripped from it, due to the tidal effects exerted by the Galactic gravitational field. Because stars in the streams follow, at first approximation, similar orbits, they can be used to reconstruct the Galactic potential at tens of kiloparsecs from the Galactic centre, providing strong constraints on the DM distribution and

---

[2]https://github.com/cmateu/galstreams
[3]http://www.astro.yale.edu/abonaca/research/halo.html

granularity even far out from the Galactic disk [49, 50, 51, 52].

A full 360° analysis of the Sagittarius stream on the sky has revealed a plethora of Galactic substructure [47, 53]. Various globular clusters, such as Palomar-12 and NGC 4147 [54, 55], have in fact been identified as belonging to the Sgr stream. While being the home to a blue horizontal branch population of stars with age ≥ 10 Gyr [56], the predominant stellar population of the Sgr stream has ages between 6-9 Gyr [57]. The ongoing accretion of Sgr and its tidal tail provide a unique insight into what the last major merger of the Milky Way may have looked like. Hence, the Sgr stream holds the power to establish a strong reference for the properties of accreted stellar populations, which is transferable to ongoing research regarding accretion history of the Milky Way.

Faint, low-mass stars that compose streams may not be visible in all wavelengths of light and are usually widely dispersed, making them hard to detect. For instance, Miskolczi et al. (2011) find 28 galaxies showing distinct stream-like features against 90 galaxies showing faint stream-like features using SDSS data release (DR) 7 [58], each with varying apparent lengths as a result of their different stages of accretion. Although streams remain somewhat mysterious to this day, understanding the origin of their stellar populations may strengthen our understanding of the merger history of the Milky Way.

However, not all stellar streams in the halo have an extragalactic origin. The Galaxy indeed also contains tens of very narrow stellar streams, more likely made of stars stripped from globular clusters, old stellar systems with typical masses of few $10^5 M_\odot$, mostly orbiting in the inner halo of our Galaxy [59, 13, 60].

1.1.3   Ancient merger debris in the MW halo

The discovery of spatially coherent structures in the halo of our Galaxy brings clues on the recent past of the Milky Way, since stars that we see nowadays in streams have possibly escaped their progenitor system very recently (typically within one billion years ago). The search for stars accreted by the Milky Way at earlier times of its evolution are more difficult to find, since stellar streams associated to early accretions are now expected to be fully mixed with the field stars and to have lost their spatial coherence. Cosmological simulations of galaxy mergers predict that the local volume of the Milky Way should contain hundreds of groups of stars with distinct kinematic properties, which are the remains of past merger events in the Galaxy. Thanks to the vast amount of high-quality data from Gaia DRs, such theories are being confirmed through observations and several halo substructures can be linked to a massive, possibly single, accretion event - the last major merger of the Milky Way, between itself and the so-called Gaia-Sausage-Enceladus (GSE) dwarf galaxy [61, 62, 63, 64, 65, 66, 67]. In particular, the first two Gaia releases have shown that the stellar halo of our Galaxy, at distances of about 10 kpc from the Galactic center, is

dominated by the GSE remnants.

Stars associated with this merger event are, on average, characterized by peculiar kinematics and chemical abundances, even if the overlap with the corresponding properties of in-situ stars is not negligible. A map by Helmi et al. (2018) of the kinematic properties of GSE tentative members is illustrated in Fig. 1.3 [61]. With a mass estimated to be between one fourth and one tenth of the mass of the Milky Way at the time of the accretion, this accretion event has marked a significant step in the evolution of our Galaxy. The Galactic disk in place at the time this merger occurred has indeed been significantly damaged by this accretion and part of its stars have been expelled at large distances from the Galaxy mid-plane, contributing to form the stellar halo. It is by studying these stars that it has been possible to date this accretion event to about 10 billion years ago [1, 68, 69, 63, 70]. There has been great excitement around this discovery and its consequences on the disk evolution and its star formation; however, the exact characteristics of this accretion (baryonic and dark matter masses of the satellite, its gas content and properties, its orbit) are still largely unknown. We still lack a model able to fully explain the properties of the satellite progenitor, Gaia-Sausage-Enceladus.

Beyond the question of the characteristics of the GSE satellite, a more difficult question lies: was the GSE-progenitor a single satellite? Or are several satellites hiding in kinematic and chemical space, embedded in the GSE region? And more generally, to what extent is the merger tree currently reconstructed from Gaia data correct and complete? The answer to this question is not trivial. From the point of view of the current observational data (Gaia and spectroscopic surveys such as APOGEE) it is not possible to disentangle the number of satellites the GSE sequence is really made of. This is why a development of new simulations of the MW-GSE-like mergers are crucial; they will allow to understand to what extent the current solution (a single massive satellite) is unique, and propose different scenarios that can be checked with future Gaia releases and with spectroscopic surveys like the WHT Enhanced Area Velocity Explorer (WEAVE), Multi-Object Optical and Near-infrared Spectrograph (MOONS) and 4-metre Multi-Object Spectroscopic Telescope (4MOST).

1.2 Dynamics of merging galaxies

What is the main reason for the galaxy mergers? First, a finite-in-size massive dwarf galaxy moving through the halo of the bigger one is a subject of dynamical friction. This dissipative force drags the dwarf galaxy towards the centre of a more massive one. The time scale of the merger thus depends on the strength of dynamical friction which heavily depends on the relative velocity of the systems and their density distributions. This process is well studied in a number of works showing how the orbit of a dwarf galaxy is affected. However, these works are mostly based on pure N-body

simulations of collisionless DM and star particles [71, 72, 65, 67].

In addition to the stellar and DM mass components, gas clouds contribute to the total mass of a galaxy. The evolution of gas during a galaxy merger is illustrated in Fig. 1.4. Unlike stars and DM, gas is collisional - that is, molecules in a gas cloud interact with each other, resulting in the exchange or radiation of energy. Subsequent hydrodynamical effects, namely gas pressure and energy dissipation via cooling, play important roles in galaxy mergers. Dynamical friction refers to the drag force that arises when a massive object (e.g. a dwarf galaxy) moves through a background of lighter objects, such as stars or gas belonging to a more massive Galaxy. This force can cause the dwarf satellite to lose kinetic energy, ultimately leading to a merger event.

Gas pressure, on the other hand, refers to the pressure exerted by a gas on its surroundings. In the context of galaxy mergers, gas pressure can stabilise the gas within a galaxy by helping to balance the gravitational forces that are acting on it; under the influence of gravity, the gas is compressed and the pressure it exerts increases accordingly, thus enabling it to counter the gravitational forces causing its compression. Once the gas pressure is equal to the gravitational force, the gas is prevented from collapsing further and the system is said to have reached hydrostatic equilibrium. Mathematically, this can be described by the Euler equation [73]

$$\frac{d\bar{v}}{dt} = -\nabla\Phi - \frac{1}{\rho}\nabla P = 0 \,, \tag{1.1}$$

where $\bar{v}$ is the velocity vector of the gas, Φ is the potential of the galaxy, ρ is the gas density and P is the gas pressure. The underlying assumption is that the net Lagrangian acceleration of the gas resulting from the sum of hydrodynamical and gravitational forces is zero.

In addition to helping to stabilize the gas within a galaxy, gas pressure can also influence the dynamics of a galactic merger. The gas in each of the merging galaxies can be subjected to different gravitational forces and can be compressed as the galaxies approach each other. This can lead to the formation of shocks in the gas, which can then transfer energy to the stars and dark matter in the galaxies, influencing their dynamics and the overall evolution of the merged galaxy.

Overall, gas pressure and microscopic radiative processes play an important role in the structure and dynamics of galaxies, and understanding the role that it plays can help us better understand the processes that shape and evolve galaxies over time. Beyond the dynamical impact of gas, the chemical evolution of galaxies is expected to be influenced by inflow, outfall or radial gas flows [74], which, by altering the gas content of a galaxy, have a direct influence on its star formation.

1.3   Project Outline

The research project aims to explore the structure of the major merger debris of a massive GSE-progenitor-like dwarf galaxy accreted onto the MW-like disk. More particularly, the aim of the project is to understand how the initial orbit of the satellite and implementation of gas and consequent star formation are imprinted in the kinematic properties of a MW-GSE-like merger, in a quest to further our understanding of the structural development of the Milky Way. We attempt to do so by developing and comparing a set of pure N-body and hydrodynamical models of pairs of galaxies with similar properties to the Milky Way and the GSE-progenitor, which are generated, run and analysed as detailed in Chapter 2 where we also list and describe in detail our chosen set of models. The main results of our analysis are presented in Chapter 3. The main results of the work are summarized in Chapter 4. By achieving so, we hope to make a step forward in understanding the presently observable kinematics and chemistry of the Milky Way and build upon previous non-hydrodynamical research on the matter (outlined throughout Section 1 and in Appendix A). The novelty of the inclusion of hydrodynamics to this analysis lays the ground work for further studies of the MW-GSE merger, which we expect to be multiplied in anticipation of coming data releases from European Space Agency (ESA)'s Gaia space mission (DR4 is expected in 2026) and the 4MOST spectroscopic survey (first data release expected in 2024-2025), and is transferable to the analysis of MW-like galaxies.
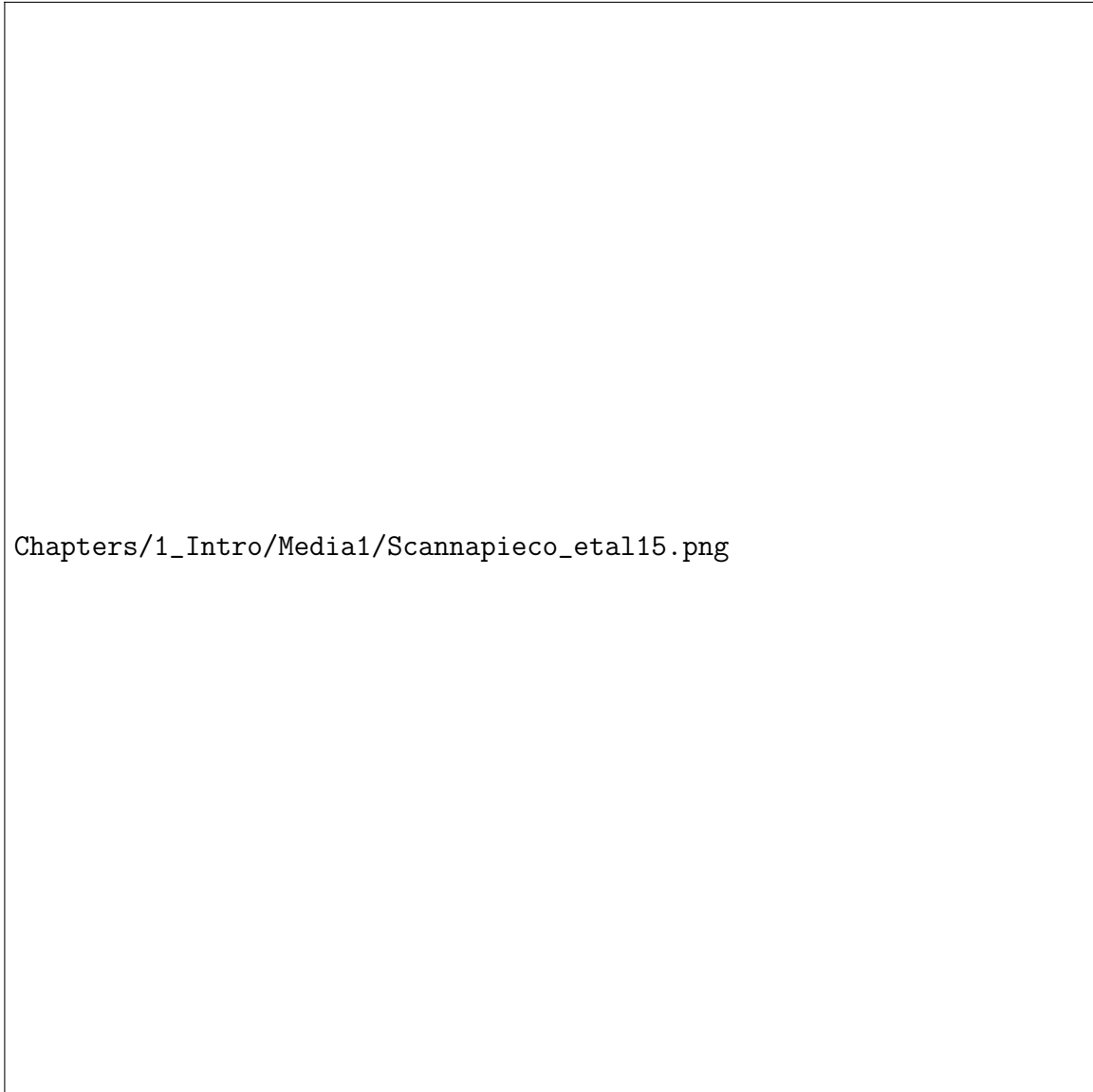
Figure 1.1: Spatial distribution of dark matter (top), gas (middle), and stars (bottom) resulting from a high-resolution simulation of the Local Group, from Scannapieco et al. (2015). Continuous circles indicate the MW candidate and dashed circles the Andromeda candidate.
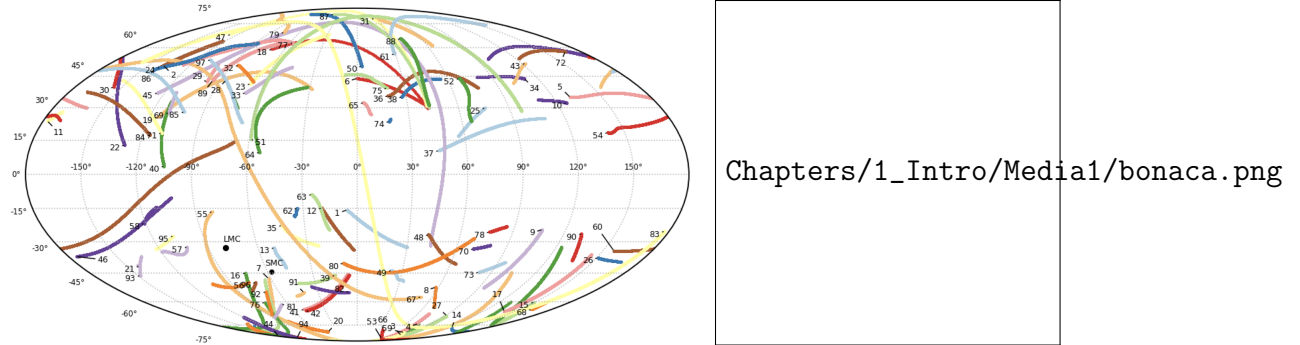
Figure 1.2: *Left:* Mollweide projection map in Galactic coordinates of the celestial tracks for the 97 stellar streams according to Mateu (2022). *Right:* several stellar streams in the MW halo (Bonaca et al. 2012).
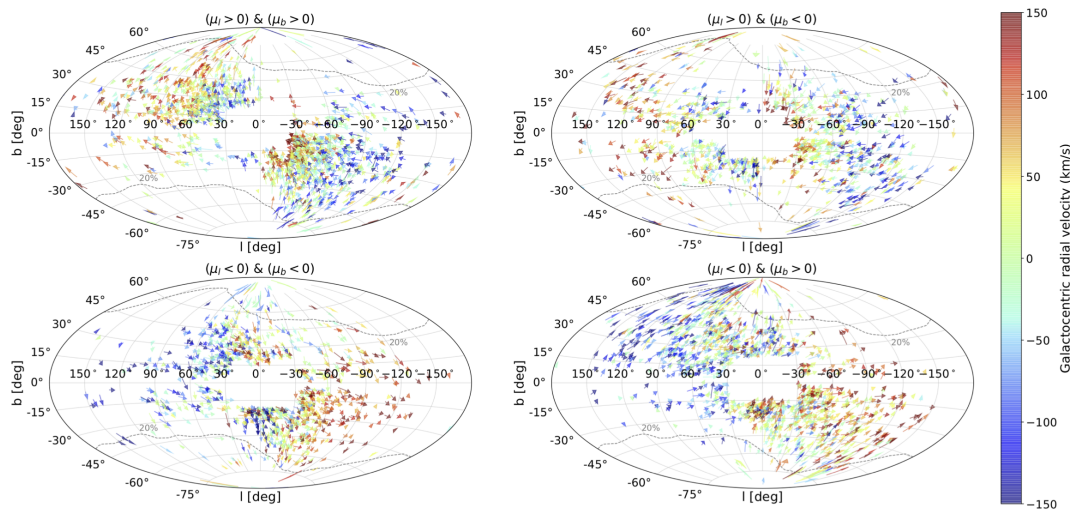
Figure 1.3: Kinematic properties of GSE tentative members on the sky from Helmi et al. (2018). The proper motions, depicted by the arrows, reveal a rather complex velocity field. A global kinematic pattern of the GSE merger debris arises because of the coherent retrograde sense of rotation of the stars in their orbits.

Figure 1.4: Evolution of gas distribution during a gas-rich MW-GSE-like merger in the x-y plane, plotted in increments of 0.4Gyr. The accreted galaxy is on a prograde orbit and contains 20% of the total gas mass of the more massive galaxy. Distinct streams of gas are left trailing behind the dwarf galaxy while both galactic disks are heavily perturbed during the merger (Marabotto et al. (in prep.)).

Chapter 2

Research Methods

The methods by which all N-body, hydrodynamical, MW-GSE-like merger models were elaborated, generated and analysed are described in this chapter. The creation and analysis of our models follows a sequential step-by-step procedure as outlined below:

1. Generation of merger models

    (a) Initial conditions generation and choice of the orbital parameters.
    (b) Numerical simulations of the galaxy mergers.

2. Analysis of the modelled merger properties

    (a) Merger orbits.
    (b) Structure of the merger debris in the total energy - angular momentum ($E-L_z$) space.
    (c) GSE disruption study via escape times calculation.
    (d) Star formation histories of the GSE and the MW.

These steps are developed in further detail in the subsequent subsections. They reflect the research methods undertook throughout this project, explaining how galaxy-pair configurations that adequately recreate a Milky Way-GSE-like merger event were developed. Data analysis of the generated simulations, as well as the generation of the files containing ICs, was carried out in Python. The final list of merger models is then described in Section 2.2.

2.1 Model generation

2.1.1 Initial conditions for simulations

In order to run a dynamical model of the galaxy mergers we first need to adopt certain properties of both galaxies (MW and GSE-progenitor) and set up the initial

Table 2.1: Constant parameters used to define the the initial conditions our our model MW-GSE-like galaxy mergers. The motivation of our analysis being the investigation of mergers with varying gas fraction, the masses of individual matter-components are not constant and are described in Table 2.2.

Galaxy	M_{Tot} [$M_\odot$]	Component	Potential Profile	Scale Parameters [kpc]
MW	3.35×10^{11}	Gas	Myamoto-Nagai	$a = 10, b = -0.06$
		Stars	Myamoto-Nagai	$a = 4.5, b = -0.4$
		DM	Plummer	$\beta = 16$
GSE	5.74×10^{10}	Gas	Myamoto-Nagai	$a = 5, b = -0.02$
		Stars	Plummer	$\beta = 0.85$
		DM	Plummer	$\beta = 2$

parameters of the GSE-progenitor orbit. These are summarised in Table 2.1. We consider the host (MW-like) galaxy to be represented by three components, including a live DM halo, and stellar and gaseous disk components. The DM distribution is considered to be a Plummer sphere [75], while the disk components are assumed to be in the form of Myamoto-Nagai density distributions [76]. These translate to the following potential profiles:

$$\Phi_P(R, z) = \frac{-GM_{halo}}{\sqrt{R^2 + \beta^2}} \, , \tag{2.1}$$

$$\Phi_{disk}(r, z) = -\frac{GM_{disk}}{\sqrt{r^2 + (a + \sqrt{z^2 + b^2})^2}} \, , \tag{2.2}$$

where G is the gravitational constant, M_{halo}, M_{disk} are the total masses of the galactic component, β is the scale radius of the halo, a and b are the scale length and the scale height of the stellar disk. Beside reducing to a razor-thin disk (see Kuzmin G.G. (1956) [77]) when $b \to 0$, the Miyamoto-Nagai potential reduces to that of a Plummer sphere when $a \to 0$. The equilibrium distribution functions for both the host galaxy and the GSE-progenitor, as well as the above galactic potentials, were adopted using the Action-based Galaxy Modelling Architecture (AGAMA) software library [78].

AGAMA is a powerful tool used to deal with arbitrary potential profiles extracted from N-body models, also capable of constructing self consistent galaxy models using galactic dynamics. For our initial conditions, each galaxy was created in isolation, then the Milky Way-like galaxy was placed in the centre of the coordinate system, while the GSE location was chosen to be far away from the centre of the host.

Since parameters of the Milky Way (mass, spatial scales of its components) are largely unknown at the time of the GSE merger, we assumed that the total mass of the host galaxy is close to the present-day one of the Milky Way. This would simply

imply that most of the Milky Way was already in place around the GSE merger. However, to inspect the manifestation of various amounts of gas, we vary its relative fraction in comparison to the total mass. In other words, we keep the masses of the Milky Way the same in all our models but redistribute it between gas, stars and DM in different models (see details in Table 2.2).

The parameters of the GSE-progenitor galaxy are even less constrained. Apart from the estimates of its total stellar and DM mass, we do not have any reliable predictions regarding its structure. Since the GSE-progenitor is a dwarf galaxy, we assume that it is also represented by DM halo, gaseous disk and stellar components. The latter is considered to be in a quasi-spherical shape.

2.1.2   Hydrodynamical simulation of galaxy mergers - GIZMO

Once the initial conditions were generated we run a full N-body/hydrodynamical simulations using a state-of-the-art GIZMO code. The GIZMO code is a flexible, massively parallel, multi-purpose smooth particles hydrodynamics (SPH)-based fluid dynamics and gravity calculation [7, 79]. Our simulations take into account radiative cooling and heating of the interstellar medium (ISM) from H and He ionization and recombination, collisional, dust collisional, free-free, molecular, cosmic ray and Compton effects from Hopkins et al. (2017) [80]. This allows us to trace some basic properties of the multi-phase ISM, including cold ($10^2 - 10^4$ K), warm ($10^4 - 10^6$ K) and hot ($> 10^6$ K) gas. Our simulations also allow the formation of new star particles from the dense ISM, which, together with the stellar feedback, were implemented following Springel & Hernquist (2003) [81]. Our simulations run over a total duration of 10 Gyr and generate a total of 100 snapshots, returning a dataframe containing 6D-positions and velocities, masses and ages of each particle after every 100 Myr time-step. In this way, we can trace the evolution of a single particle or of the system as a whole.

2.2   Simulations analysis

Using the output snapshots from the ran simulations, we carry out an analysis of the MW-GSE-like galaxy mergers. We illustrate an example of the evolution of the merger system in Fig. 2.1. A primordial step in the data analysis is to recenter the system to the center of the MW; as the simulation advances in time, the position of the MW is moving through the computational domain due to gravitational attraction from the massive GSE-progenitor. To counter this, we implement a routine to recenter the coordinate system to the center of the Milky Way at all times in order to ensure that we remain in its restframe. This will largely simplify our calculations and the elaboration of boundary conditions for indexing and particle selection later in
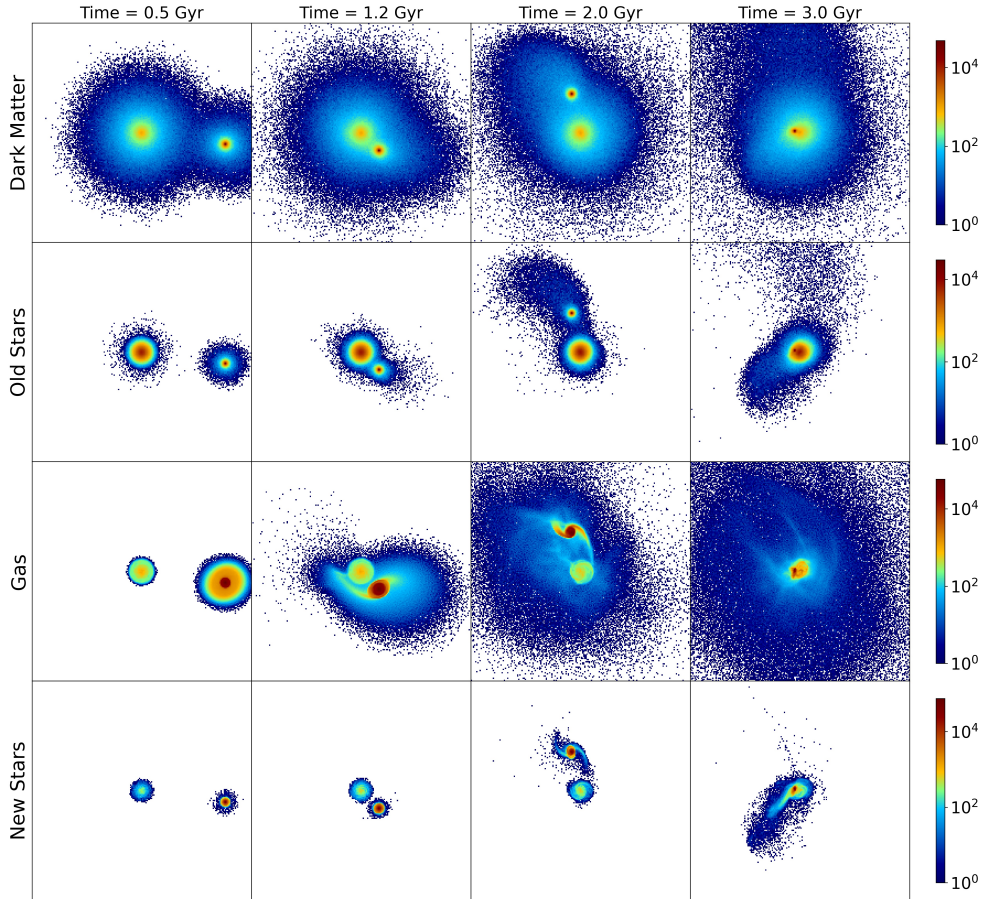
Figure 2.1: Evolution of the system similar to Fig. 1.1, this time showing an example model from our simulations. From top to bottom, the distribution of DM, pre-existing stars, gas and newly formed stars are shown for different times before the full coalescence of the Milky Way and the GSE-progenitor. In all panels, the Milky Way is located in the centre. The linear size of one square panel is 400 kpc.

the analysis, namely being an essential implementation to the calculation of galactic potentials, the angular momentum of particles and other parameters of the system.

In order to disentangle particles belonging to either the Milky Way or to the GSE-progenitor across different snapshots, we used the initial snapshot to spatially dissociate particles from the Milky Way and the GSE-progenitor. This is done by identifying the particle IDs for DM or pre-existing star components found within (MW) or beyond (GSE) 100 kpc of the Milky Way center. We do not explicitly trace the gas particles because of the collisional nature of the ISM.

Newly formed stars however require a more advanced approach in their association with the main galactic systems in the simulations. In particular, in the association of newly formed stars with either the MW or the GSE-progenitor, we rely on revised

spatial selections, which we describe in Sect. 2.2.4.

2.2.1 Merger Orbit

We seek to trace the evolution of the GSE-like satellite as it merges with the Milky Way, comparing how the orbit changes as we modify the initial 6D kinematic properties of the GSE progenitor, as well as the gas fraction of both galaxies. To map out the orbit, we calculate the distance of the center of GSE to the center of the Milky Way. We can locate the respective galactic centers by finding the mean positions $(\bar{x}, \bar{y}, \bar{z})$ of all particles belonging to the Milky Way or to GSE in the dataframe. We then calculate the 3D galactocentric distance of GSE-progenitor as follows:

$$R = \sqrt{(\bar{x}_{GSE} - \bar{x}_{MW})^2 + (\bar{y}_{GSE} - \bar{y}_{MW})^2 + (\bar{z}_{GSE} - \bar{z}_{MW})^2}, \qquad (2.3)$$

where $\bar{x}_{GSE}$, $\bar{y}_{GSE}$, $\bar{z}_{GSE}$ and $\bar{x}_{MW}$, $\bar{y}_{MW}$, $\bar{z}_{MW}$ are the Cartesian coordinates of the centres of the GSE-progenitor and the Milky Way, respectively. Recall, however, that the center of our coordinate system is associated with the center of the Milky Way.

Depending on the parameters of the system (initial velocity of the GSE-progenitor, total mass, its relative gas fraction), we notably expect a different time scale (time until the coalescence of galaxies) of the merger. In particular, the most interesting effect is expected once we include a substantial amount of gas in our systems. This effect is largely unexplored in the context of the MW-GSE-merger investigation, partially because the gas content of the GSE-progenitor is unknown, despite suggestions that it was a gas-rich dwarf galaxy [82].

2.2.2 $E-L_z$ phase space

Numerous studies have indeed suggested that the imprints of past merger events, even if dispersed in configuration space, should still be identified in kinematics-related spaces such as the $E-L_z$ phase-space. For example, it has been suggested that distinct accreted satellites should appear as coherent structures in the $E - L_z$ space [83] and that the shape of these structures should not significantly change during the accretion event, even in the case of a time-dependent potential [84, 36, 85]. From the number of substructures found in the $E - L_z$ phase-space, it should be possible to set a lower limit to the number of past accretion events [83, 85]. However, it is still necessary to check whether this search is really feasible and meaningful, namely to investigate the significance of structures identifiable in the $E - L_z$ phase-space.

Therefore, the predominant physical quantities we refer to in our merger analyses are the total energy (E) and a z-component of the angular momentum (L_z):

$$E = \Phi + \frac{1}{2}(v_x^2 + v_y^2 + v_z^2) \; [\text{km}^2 \; \text{s}^{-2}], \qquad (2.4)$$
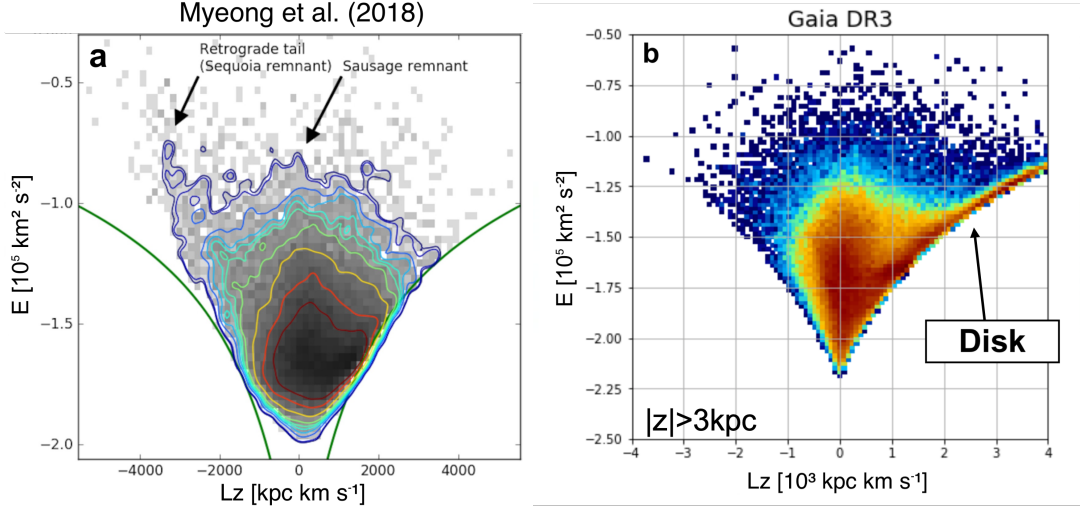
Figure 2.2: a) Distribution in $E - L_z$ phase-space of Milky Way halo star sample of Myeong et al. (2019). They find two populations of merger debris; one radial population with low L_z, which they associate to GSE, and one retrograde component which they link to a separate merger remnant, Sequoia. In the top panel, they show the L_z distribution function for stars with $E > -1.1 \times 10^5$ km^2 s^{-2}. b) Illustration of the $E - L_z$ space for a sample of SNd stars in Gaia DR3. Two main features are seen in the distribution: non-rotating GSE component around $L_z \approx 0$ and prograde rotating disk component.

$$ L_z = (-v_x y + v_y x) \left[\text{kpc km s}^{-1}\right], \tag{2.5} $$

where x, y are the Cartesian coordinates and v_x, v_y, v_z are the velocity components of particles, Φ is the gravitational potential (see Section 2.1.1 for computation method).

Since for various types of analysis we need to know the potentials of the GSE and the MW systems separately, we use the AGAMA software to calculate the potentials (Φ) using a combination cylindrical and spherical spline functions. In this case the potential is represented as a sum of azimuthal Fourier harmonics with coefficients of each term interpolated on a scaled 2D grid in the $R - z$ plane. It is restricted to models with finite density at their spatial origin, all the while spanning a broad dynamical range thanks to its near-exponential grid spacing at large radial values (see section A.4.2 in the documentation for further details) [78]). Due to the nature of our models, namely representing a system containing two galaxies of finite density with galactic halos extending to galactocentric distances as large as 100 kpc, AGAMA's approach was evidently considered to be a very efficient method for the computation of the potentials of different components in our simulations.

In the following, we seek to determine the importance and influence of gas on

the orbital properties of the merger, notably its impact on energy dissipation, by understanding how the merger debris is imprinted in $E - L_z$ phase space. At first, such analysis may be used to supplement our previous (purely spatial) analysis of the merger orbit and test the reproducibility of our models in $E - L_z$ phase-space. It is indeed easy to extract the orbital properties (prograde, radial, retrograde) of the merger debris based on the density distribution of particles along the angular momentum axis.

Different populations of merger debris can therefore be uncovered according to their kinematic properties, as illustrated Fig. 2.2. In panel **a**, Myeong et al. (2019) in fact find two distinct remnants in $E - L_z$ phase-space for the Milky Way stellar halo, one of which they associate to the GSE merger [86]. They however argue the existence of a second accretion event with retrograde debris, Sequoia, which occurred independently to the accretion of GSE [1, 69, 87]. This is concurrent with previous studies that suggest the retrograde components of the Milky Way halo originate from accreted populations, eg see Beers et al. (2012) [33], Majewski et al. (2012) [88].

In panel **b**, we show a sample of solar neighbourhood (SNd) stars extracted from Gaia DR3 [89]. We select stars with radial velocities and only include stars observed away from the mid-plane ($|z| > 3$ kpc) of the Milky Way in order to reduce a contamination from the disk stars. We clearly identify a prograde branch, which represents the Milky Way thin disk, and a radial population associated to the GSE debris, thus illustrating the power of $E - L_z$ space in uncovering remnants of merger debris in the Galactic halo.

Through our analysis, we investigate which features of $E - L_z$ phase-space are reproduced by hydrodynamical simulations. We namely seek to verify whether the particular features of the Milky Way post-merger can be reproduced, or if embedded populations in the merger debris can be identified in our MW-GSE- like merger models.

2.2.3   Escape time of the GSE stars

The assumption regarding coherency of the merger debris in kinematic space works perfectly for low-mass stellar streams, which are scattered across a large volume around the Galaxy and still observed as a distinct clump, e.g. in energy-angular momentum space $(E - L_z)$ [83]. However, for accreted systems with total masses larger than $> 10^9 M_\odot$, this coherency is no longer applicable [90, 91, 92]. This can be understood because the progenitor galaxy, as it orbits in the Galactic potential, loses part of its orbital energy and angular momentum due to dynamical friction, consequently decaying towards the potential well of the Milky Way as the merger proceeds. Stars lost in the first phases of the merger process will thus tend to have larger energies than stars lost in the final phases of the accretion events, which will tend to be more tightly bound to the Milky Way. One can expect that stars lost by the GSE-progenitor at the early stages of the merger occupy different regions of the

$E - L_z$ space compared to those captured by the Milky Way at later times. Therefore, one important parameter to be used in our analysis is the time when a given particle is no longer associated with the GSE-progenitor.

The escape times of particles were computed in order to better envision the modelled mergers. In particular, the escape time of a given particle i was defined as the time at which it becomes unbound from the GSE progenitor, namely the time at which its energy is positive in the reference frame of GSE:

$$t_{esc} = t(E_{i,GSE} > 0). \tag{2.6}$$

To calculate escape times, we develop an algorithm that works backwards in time, starting from the final snapshot in our simulations. In this special scenario, we are required to work from the GSE reference frame; due to the nature of our boundary conditions, we must work using the gravitational potential of the GSE. We recenter the system to the satellite galaxy and calculate the energy of its stars using the gravitational potential of the dwarf satellite, not that of the Milky Way, in order to identify those that are unbound from GSE. For every star within a given snapshot, we check whether 2.6 is met. If this is the case, we assign the snapshot number to the escaped star. If not, we repeat the test for the earlier snapshot, until we reach t=0. We then save the times of escaped stars back into the original dataframe. Those that never escape (as well as those belonging to the Milky Way) are saved as 'NaN' in order to for the "escaped" data array to match the length of the full dataframe when these are concatenated. We generate two data arrays for escaped particles; one containing stars only, and another looking at all collisionless particles.

Although we do not treat this in our analysis, it could be interesting to implement this algorithm to the Milky Way in order to investigate if this transfer of particles occurs in both directions, namely if the GSE-progenitor accretes a comparable amount of matter from the Milky Way to what it loses. Due to the much larger gravitational potential of the Milky Way, we however assume that this is not the case.

We can then analyse the escape times distributions and investigate the stages of the merger during which Milky Way most actively strips matter from GSE. We can further map out escape times into $E - L_z$ phase-space, notably allowing us to envision how the kinematic distribution of particles during and after the merger relates to their time of accretion.

2.2.4   Star formation history

The novelty of this project is the introduction of the analysis of star formation rates (SFRs) for our Milky Way-GSE-like merger simulations. Beyond its impact on the merger debris structure and the accretion timescale, the presence of gas is essential in initiating star formation in a galactic system. Therefore, the implementation of gas to our system of galaxies naturally allows us to investigate the conditions and properties of the birth of new stars in our merger simulation. Through analysis of

the star formation history (SFH) of both galaxies, we seek to investigate how the changing gas fraction across our models is imprinted in the form of starbursts and whether distinct populations of new stars can be identified.

As we have already mentioned, the association of new stars to the Milky Way or to GSE is however somewhat more complex than for other kinds of particles. We therefore develop a pipeline which associates new stars to the Milky Way or to GSE depending on its birth radius. In a similar manner to that described in Section 2.2.3, we work back from the final snapshot in the simulation, this time to find the snapshot at which a star is born. In this snapshot, we start by calculating the position of the GSE center from the center of the MW. The galactocentric distance of the newborn star is then computed, which we refer to as its birth radius R_1. We then find the distance between R_1 and GSE, which we call R_2. We then simply say that, at the time of formation, if $R_1 < R_2$ then the star was born in the Milky Way, whereas if $R_1 > R_2$ the star was born in the GSE.

Therefore, stars formed closer to the centre of the GSE-progenitor are associated to the dwarf satellite; otherwise, we assume that these star particles belong to the Milky Way. This simple approach perfectly works at the early stages of the evolution of the system (which only contains the two galaxies) while the GSE-progenitor is far away from the GSE centre. At the latest stages of the merger, close to the coalescence of the galaxies, this may result in some confusion; for instance, once the GSE-like satellite has penetrated the vicinity of the Milky Way, in-situ star formation in the Galactic stellar halo may overlap with star formation occurring in the GSE satellite. In this case, a new star which seemingly belongs to the MW may wrongly be associated to the GSE progenitor. Whether the passage of GSE in fact has an influence on the birth of said star or not is a question to keep in mind, of which the effects and implications could be explored in further studies.

However, the very last stages of the merger are quite short and do not significantly affect our conclusions regarding the structure of the GSE merger debris in the simulations. Therefore, assume that a purely spatial selection described here is sufficient in associating new stars to either the Milky Way or to GSE.

2.3 Models description

In this section, we provide the exact parameters of the galaxies and the initial velocity vector of the GSE-progenitor in our models. In total, we successfully ran and analysed 24 models (12 low- and 12 high-resolution, which are identical with respect to their physical parameters) with different initial conditions. A final list presented in Table 2.2 was generated as outlined throughout this chapter. The main interest of these models is to analyse the properties and orbits of a MW-GSE-like galaxy pair merger as a function of the gas fraction. Below we discuss the initial conditions for our galaxy models and the chosen parameters for our simulations, namely the gas amount inside the Milky Way and GSE-progenitor and the orbital properties of the dwarf satellite.

The first three models in Table 2.2 correspond to pure N-body simulations, i.e. without any gas particles and, thus, no star formation was considered. Referring to these three models will allow us to highlight any changes in merger properties induced by the introduction of hydrodynamics to N-body simulations. They only differ from each other in terms of the initial velocity vector. In particular, we study the evolution and structure of the merger debris in case of prograde, radial and retrograde orbits of the GSE-progenitor. In the prograde (retrograde) simulations, the direction of the merger is along (against) the rotation of the Milky Way, while we study a merger with no initial angular momentum in the plane of the MW galaxy in the radial simulation. In these cases, the initial velocity components of the GSE-progenitor are defined as follows:

- Prograde merger: $\boldsymbol{V_0} = (42, 42, 22)$ km s^{-1}

- Radial merger: $\boldsymbol{V_0} = (-59, 0, 22)$ km s^{-1}

- Retrograde merger: $\boldsymbol{V_0} = (-42, -42, 22)$ km s^{-1}

Other sets of models presented in Table 2.2 follow the same idea (prograde, radial and retrograde simulations) but differ from each other by the masses of the DM, gas and stellar components. Note that the exact discrimination between stellar and DM particles is not critical because their impact on the evolution of the system is seen only via gravitational forces. Due to its interesting kinematic properties in relation to the presently observed Galactic halo, as we will show later, we favour Model 21 when investigating individual models.

2.3.1 Resolution study

Before proceeding to a full analysis of the MW-GSE-like merger, we carry out a preliminary resolution study. The aim of this analysis is to explore the effect of the

Table 2.2: List of generated models for analysis of the MW-GSE-like mergers. Initial galactic masses for individual components (gas, stars and DM) of both Milky Way and GSE-progenitors are shown. The stellar and DM masses are altered alongside the gas mass such that $M_{Tot,MW} = 3.35 \times 10^{11}$ and $M_{Tot,GSE} = 5.74 \times 10^{10}$ are always constant. $\boldsymbol{V_0}$ is the initial velocity vector in the Cartesian coordinate system of the GSE dwarf galaxy relative to the center of the Milky Way, where the dwarf galaxy is placed at $\boldsymbol{R_0} = (187$ kpc, 0, 0). Models in brackets are analogous to their adjacent model, but are generated in high resolution, which we prioritise for our analysis. The differences between Low and High-resolution models, namely the numbers of particles for each matter component in both the MW and GSE, are outlined in Table 2.3.

Model	$M_{g,MW}$ 10^{10} M$_\odot$	$M_{g,GSE}$ 10^{10} M$_\odot$	$M_{s,MW}$ 10^{10} M$_\odot$	$M_{s,GSE}$ 10^{10} M$_\odot$	$M_{DM,MW}$ 10^{10} M$_\odot$	$M_{DM,GSE}$ 10^{10} M$_\odot$	$\boldsymbol{V_0}$ km s^{-1}
1 (13)	0	0	6.30	0.244	27.2	5.49	42, 42, 22
2 (14)	0	0	6.30	0.244	27.2	5.49	-59, 0, 22
3 (15)	0	0	6.30	0.244	27.2	5.49	-42,-42, 22
4 (16)	4	0	5.56	0.244	23.9	5.49	42, 42, 22
5 (17)	4	0	5.56	0.244	23.9	5.49	-59, 0, 22
6 (18)	4	0	5.56	0.244	23.9	5.49	-42, -42, 22
7 (19)	4	0.8	5.56	0.210	23.9	4.73	42, 42, 22
8 (20)	4	0.8	5.56	0.210	23.9	4.73	-59, 0, 22
9 (21)	4	0.8	5.56	0.210	23.9	4.73	-42, -42, 22
10 (22)	4	4	5.56	0.074	23.9	1.67	42, 42, 22
11 (23)	4	4	5.56	0.074	23.9	1.67	-59, 0, 22
12 (24)	4	4	5.56	0.074	23.9	1.67	-42, -42, 22
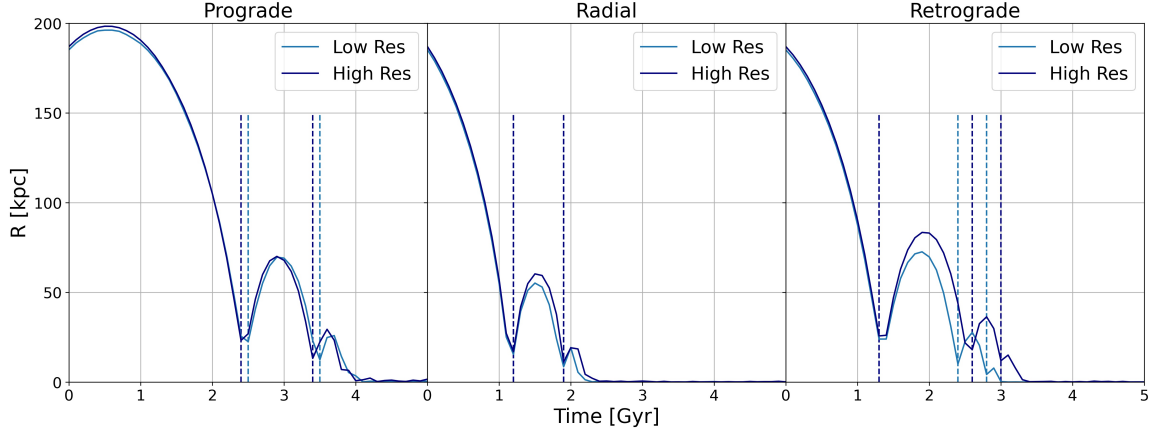
Figure 2.3: Effect of resolution on the orbital decay of accreting GSE-like dwarf onto the Milky Way-like disk galaxy. The evolution of the orbit as modelled by low (high) resolution simulations is shown in blue (navy), with annotated pericentric passages. Although the resolution affects the orbital evolution of GSE, the effect is rather small, suggesting that even relatively low-resolution simulations are capable to trace the dynamics of the system. In the retrograde case, the orbit is more sensitive to the increased resolution due to the larger number of gas particles, consequently enhancing the dynamical effects discussed in Section 1.2.

Table 2.3: Summary of the resolution study, illustrating how the number of particles n for each component of both galaxies differs at low and high resolutions. In the case of models illustrating gasless galaxies, N_{Gas}=0.

Resolution	Galaxy	N_{Stars}	N_{Halo}	N_{Gas}
Low	Milky Way	5×10^4	5×10^4	1×10^4
High	Milky Way	5×10^5	5×10^5	1×10^5
Low	GSE	1×10^4	2.5×10^4	1×10^4
High	GSE	1×10^5	2.5×10^5	1×10^6

finite number of particles, and thus the mass resolution of our N-body simulations, on the evolution of the system.

The different properties between Low and high resolution models are outlined in Table 2.3. Containing fewer particles, low resolution models are generated much faster in GIZMO and require less run-time during the data analysis of the resultant merger models. However, the increased number of particles in high resolution models improves the statistics of our N-body systems by providing a larger data sample per analysed bin for any given property.

Although we do not quantify this statistical refinement, we show in Figure 2.3

23

that there is good convergence of the results between high and low resolution models through the orbital decay of GSE. Therefore, we confidently use low resolution models to test the models and algorithms for data analysis developed throughout this chapter, of which the results are successfully applied to high resolution models. We then illustrate our final results in high resolution, minimising the random scatter in our data and reducing any statistical error thanks to the increased number of particles.

A good agreement for low and high resolutions illustrates the strong behaviour of GIZMO in providing robust results in the regions sparsely populated with particles, which is important in the analysis of the low-density environment of the stellar halo. We therefore deem this resolution study sufficient in ensuring the accuracy of our results, which are presented in the following chapter.

Chapter 3

Results

Using our set of the high-resolution simulations described in the previous Chapter, we explore not only the structure of the GSE-like merger debris after the accretion but also its evolution over time, which in our models is affected by the orbital parameters of the merger and by the gas content of both the central MW galaxy and the GSE-progenitor. Although, we run all the simulations for 10 Gyr, all the mergers are fully complete within < 5 Gyr. Therefore, when discussing the latest stages of the merger, we refer to 5 Gyr, unless it is specified in the text.

Using our set of high-resolution simulations described in the previous Chapter, we explore the structure of the GSE-like merger debris and its evolution over time. In our models, these are affected by the orbital parameters of the merger and by the gas content of both the central Milky Way galaxy and the GSE-progenitor.

3.1 Merger time scale and orbit of GSE

We begin by taking a look at the merger time scale of the GSE-progenitor across our models. From studies of the kinematic properties of the local stellar halo, the merger of GSE with the Milky Way is estimated to have occurred $8 - 11$ Gyr ago [1, 63, 68, 69, 70]. Therefore, one can naturally expect that that the GSE-progenitor evolved in "isolation" for $< 3 - 6$ Gyr since the formation of its proto-halo. A direct way to find the merger time scale is to find the moment of the full coalescence of the Milky Way and the GSE-progenitor by analysing the orbital evolution of the dwarf satellite during its infall.

A closer look at the pericentric passages during the orbital decay of Model 21, as well as its orbital path in 2D space, is detailed in Fig. 3.1. Recall that this model assumes a retrograde infall of the GSE-progenitor. In panel **a**, we highlight the pericentric passages of GSE as displayed in Model 21, found to be $R_p^1 = 25.8$ kpc, $R_p^2 = 18.1$ kpc and $R_p^3 = 11.9$ kpc, respectively. These reflect the rapid change in the rate of the GSE infall as it approaches closer to the center of the Milky Way, where
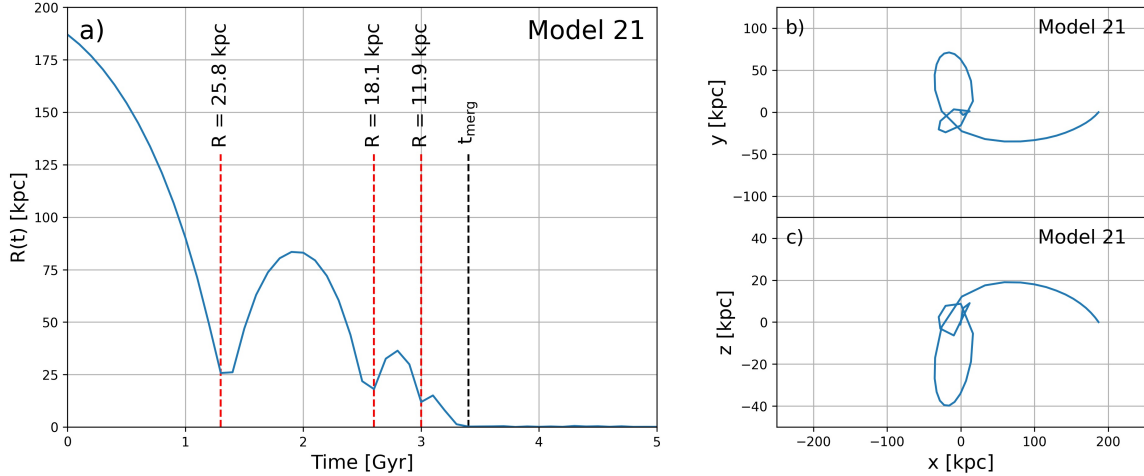
Figure 3.1: **a)** Orbital decay of the GSE satellite as simulated in Model 21, showing the galactocentric distance of GSE from the Milky Way as a function of time. In red, the pericentric passages mark the smallest separations between the two galaxies during the approach of the GSE-like satellite. These are found from the local minima in the orbit of GSE up until the time of the merger. The coalescence time for this model is 3.4Gyr, with the black dashed line marking the time of the merger t_{merg}. On the right, we illustrate the orbital path of the GSE satellite in **2D** space for Model 21. To trace the spatial coordinates of GSE, we define its center as the mean position of its stars relative to the center of the Milky Way, which itself lies at the center of our coordinate system. In **b)** we trace the accretion of the GSE in the $x - y$ plane. In **c)**, a similar plot is projected onto the $x - z$ plane.

its gravitational potential is most influential. This is also illustrated in panels **b** and **c**, where we easily visualise the rapid decline of the orbit during its later stages.

As one can see in the figure, the merger is fully completed after ≈ 3.4 Gyr of evolution of the system. We define the time of the merger, t_{merg}, as the snapshot in our simulations at which the mean position of all particles belonging to the GSE satellite is zero. As we define the center of the Milky Way at the origin of our coordinate system at all times, this implies that the position of the center of GSE is the same as the position of the center of the Milky Way at and beyond $t = t_{merg}$. Hence, the mean position of all particles in the system after completion of the merger is always $\bar{R}_{tot} = 0$. Note that the coalescence of the galactic centers does not imply the end of the evolution of the merger debris; the coalescence of the outer parts, as well as any tidal features, may occur on longer time-scales. Nevertheless, most of the GSE-progenitor mass has reached its final destination, the center of the Milky Way, at $t = t_{merg}$.

In Fig. 3.2 we show the evolution of the galactocentric distance from the Milky Way center to the GSE-progenitor galaxy. The compact orbital curves of radial
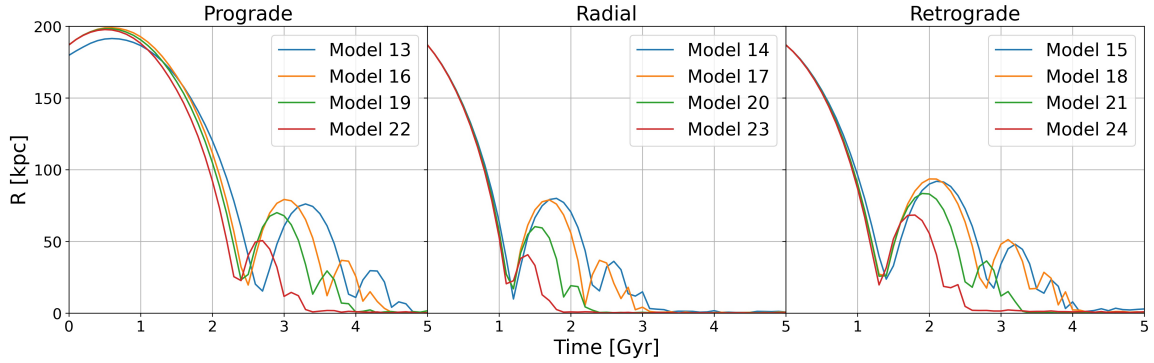
Figure 3.2: Comparison of the orbital decays of the GSE satellite across all high resolution models, showing the changing distance of GSE from the Milky Way center over the span of 5 Gyr. Beyond the coalescence time, $R(t)$ is naturally null. From left to right: prograde, radial and retrograde models are grouped into respective panels. Increasing the gas fraction of the system causes a noticeable 'dampening' of the orbit of GSE. We also notice a decreasing number of pericentric passages of the orbit in correlation to the increasing gas fraction, indicating an accelerated infall for a GSE progenitor with a heavier gas component

merger models depict the sudden deceleration undergone by the satellite following its head on collision. This is a rather intuitive finding, as the gravitational force exerted by the Milky Way acts in parallel to the line of motion of the GSE progenitor at all times, that is, in the exact opposite direction to the motion of the satellite. Thus, the deceleration of GSE is maximised and its orbit is quashed, leading to tighter pericentric passages and a faster time of accretion. We also show that retrograde models have shorter timescales than their prograde analogues, which we explain from the the contribution of the dynamical friction experienced between the counter-rotating gaseous components in decelerating the GSE-progenitor.

The change in gas fraction across models is also found to have a flagrant effect on the MW-GSE-like merger. The impact of gas fraction on the merger orbit as a whole is observable across all panels of Fig. 3.2, regardless of the initial velocity of the satellite. The amount by which the orbital decay of the GSE-like satellite is quenched with increasing gas fraction is comparable between prograde, radial and retrograde models; although the orbits are affected by changing gas fraction, the quantity by which they differ is consistent across all three sets of models. The pericenters of the orbits occur earlier in the simulations containing a more massive gas component in the GSE-like satellite, while the distance of the apocenters is concurrently reduced.

By categorising our merger models according to the orbit of the GSE satellite, we are able to investigate the effect of gas fraction between the proto-galaxy representing the Milky Way and the GSE-like progenitor on the merger time. This is illustrated in Fig. 3.3. To do so, we select our high resolution models with non-zero total gas
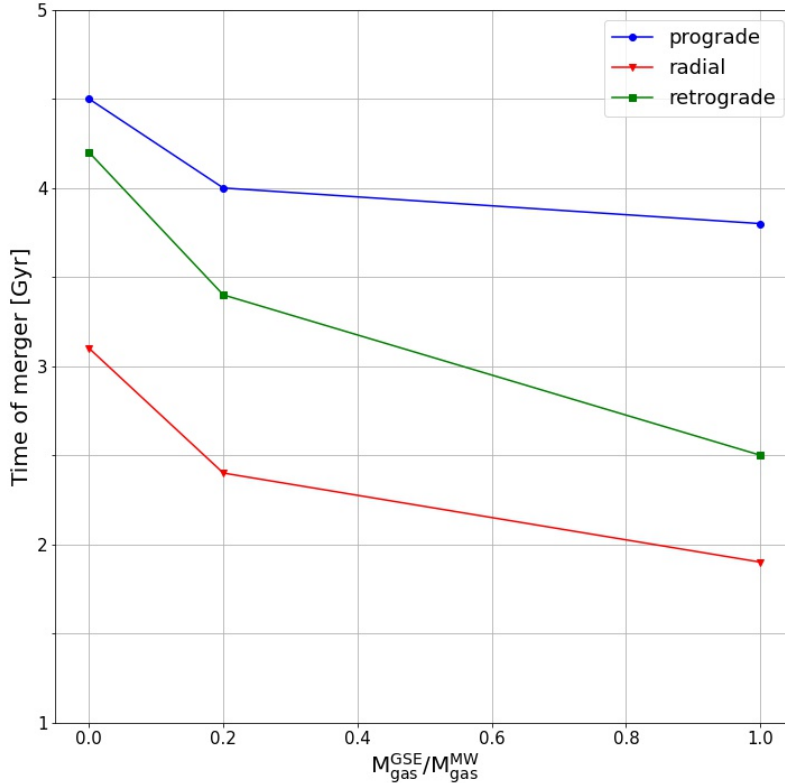
Figure 3.3: Time of the galaxy merger as a function of the relative gas fraction in the GSE and the MW galaxy, excluding gasless models. All three sets of models have identical Milky Way gas mass, $M_{gas}^{MW} = 4 \times 10^{10} M_\odot$. Different colours show the merger time for three types of orbits: blue (prograde), red (radial) and green (retrograde) (see orbital parameters in Table 2.2). For models with identical gas fractions, the accretion event is concluded quickest in a scenario involving a head on collision between both galaxies. Across models with identical orbital properties, those with a lower gas fraction demonstrate a later completion of the galaxy merger.

mass (Models 16-24, see Table 2.2), implying that M_{gas}^{MW} is fixed at $4 \times 10^{10} M_\odot$. We find that the merger event occurs at earlier times for models containing a more massive gas component in the GSE progenitor, elucidating the effects of dynamical friction hinted by the trends in the orbital decays. We also notice that the decrease in t_{merg} is more prominent between two models respectively simulating a gasless GSE ($M_{gas}^{GSE}/M_{gas}^{MW} = 0$) and one containing gas ($M_{gas}^{GSE}/M_{gas}^{MW} = 0.2$) than between two models containing gas rich GSE progenitors; despite the drastic increase in gas fraction to $M_{gas}^{GSE}/M_{gas}^{MW} = 1$, amounting to a gas mass ratio increase larger by a factor of five compared to the previous models, t_{merg} is less affected for prograde and radial mergers. This illustrates the impact that the introduction of dynamical friction has on the galaxy merger - gas in the GSE progenitor collides with that of the Milky Way
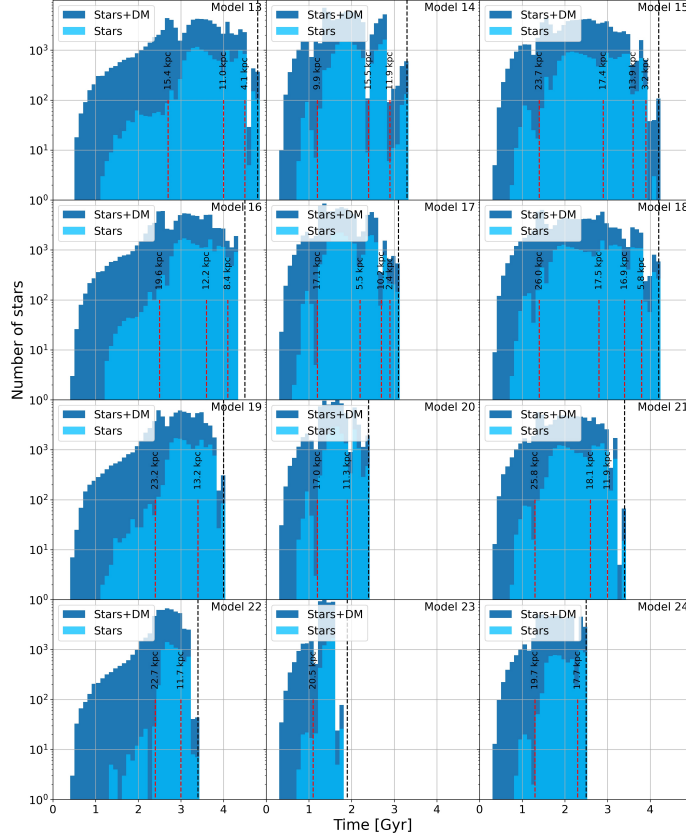
Figure 3.4: Distribution of the escape times of star and DM particles belonging to GSE. In light blue, the distribution obtained when isolating pre-existing GSE stars from DM is over-plotted. New stars formed during the accretion event are not included. The pericentric passages of GSE are shown using red dashed lines, the merger time in black. Bursts in the number of escaped particles coincide with the pericentric passages of the GSE orbit, where the gravitational force exerted by the Milky Way on GSE is strongest.

proto-galaxy, enhancing the deceleration of the satellite and accelerating its accretion.

This is further illustrated in the retrograde case. With the infall of GSE acting against the rotation of the Milky Way disk, the angular momentum of GSE is more abruptly radialised. We therefore notice that a GSE progenitor on a retrograde orbit is more sensitive to an increase in gas fraction, with a decrease in merger time between models 18 (gasless-GSE, $M_{gas}^{GSE}/M_{gas}^{MW} = 0$) and 24 (gas rich-GSE, $M_{gas}^{GSE}/M_{gas}^{MW} = 1$) of 1.7Gyr. In contrast, the equivalent decrease in t_{merg} is only 0.7Gyr in the prograde case, with the effects of dynamical friction being significantly less impactful due to the coherence between the net angular momenta of both galaxies. The radial case lays the middle ground with a change in t_{merg} of 1.2Gyr.

In order to understand the implications the orbital path of the GSE-like satellite
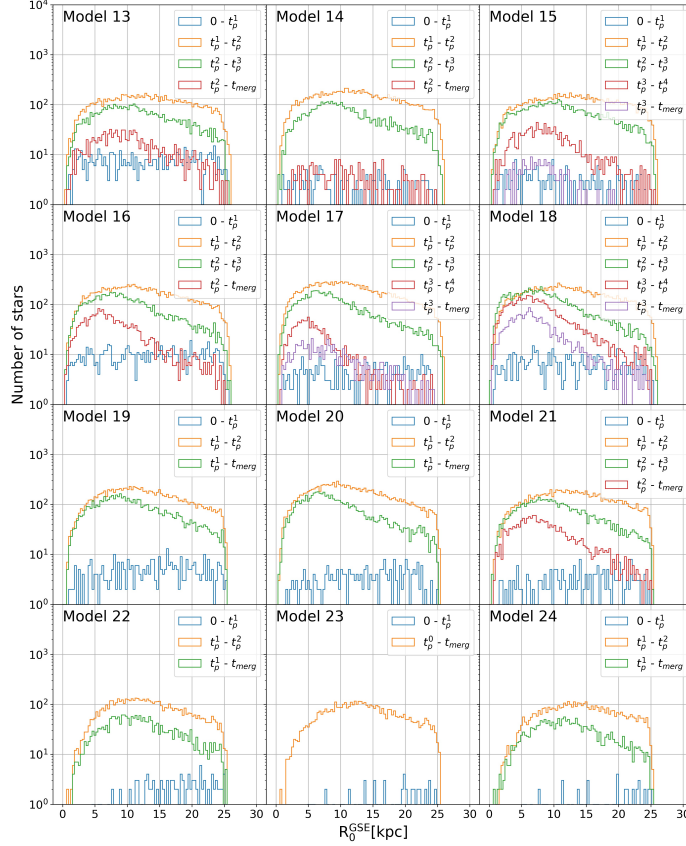
Figure 3.5: Escape time distributions of GSE stars as a function of their initial distance from its center, R_0^{GSE}, categorised according to their escape time in relation to the pericentric passages of the orbit. The largest fraction of escaped stars are stripped from GSE between the first and second pericentric passages of its orbit across all models, suggesting that the accreted satellite is most perturbed after its first approach within the vicinity of the Milky Way.

during its accretion, we now focus our analysis on the escape times of particles belonging to the dwarf galaxy. The escape time of a given particles is defined using Equation 2.6. We notably search for correlations between the pericenters of the orbit and the number distribution of escaped particles, illustrated in Fig. 3.4.

The simulations show a gradual increase in the number of escaped stars as the satellite first approaches the Milky Way. We then find peaks in the number distribution of escaped stars between each pericentric passage of the orbit, with most stars being stripped from the GSE-like progenitor at times between the first (t_p^1) and second (t_p^2) pericentric passages of its orbit. This is further developed in Fig. 3.5, where we show that this is true across all models. This is partly due to the increasing strength of the gravitational potential of the Milky Way at lower galactocentric radii. Although we could expect the pericenters to correspond exactly to the peaks of es-

caped particles, we do note a slight lag between the closest approach of GSE and the greatest loss of stars. Stars are dragged out of the GSE potential as the dwarf galaxy starts travelling away, which could be what we observe today between the Milky Way and Sgr as stellar streams.

We also deduce from Fig. 3.5 that a very small quantity of stars escape the GSE-like progenitor prior to its first pericentric passage, implying that not many stars stars are stripped from GSE during its approach; they are mainly stripped when the potential of the Milky Way acts against its line of motion. The radial distribution of the escaped stars between the first and second pericenters is rather smooth, with a consistent peak at $R_0^{GSE} \approx 10 - 12$ kpc in all models. One may find this value surprising, as we would intuitively expect the majority of escaped stars to come from the outskirts of the GSE-like satellite given that this is where the galactic potential of GSE is weakest, meaning its stars are less bound. However, the outskirts of the GSE galactic disk are less densely populated than the inner disk and bulge, implying that the number of stars within 10-12 kpc from the center of GSE is significantly greater than beyond 12 kpc.

This suggests that the GSE halo indeed has the highest fraction of escaped stars while explaining why the total number of escaped particles is highest at a closer galactocentric radii than one could expect. It is also clear that stars within $10-12$ kpc of the GSE center are too strongly bound to the dwarf galaxy to be stripped by the gravitational potential of the Milky Way in large amounts.

During the later stages of the merger, we see this peak shift to smaller values of R_0^{GSE} as the pericenters of the GSE orbit get closer to the Milky Way and notice a decrease in the escaped stars number distribution. Despite the stronger gravitational force exerted on the GSE-like progenitor, the most loosely bound stars have already escaped GSE and the Milky Way is required to 'dig deeper' into the potential well of the dwarf galaxy to accrete more stars.

3.2 Evolution of total energy and angular momentum

As discussed in the Introduction, various kinematic characteristics of stellar mergers debris are used to identify accreted stellar populations and describe the properties of their progenitor galaxies. The most commonly used are so-called integrals of motions, or the total energy E and the angular momentum, in particular its L_z component. Both of these quantities are believed to be conserved during the merger, thus allowing to trace the origin of different structures in the stellar halo [24, 83]. Prior to the analysis of the energy-angular momentum space, we test whether the widely-used assumption regarding the conservation of energy (E) and azimuthal angular momentum (L_z) is reasonable in our simulations.

Fig. 3.6 shows the evolution of the angular momentum component across all simu-
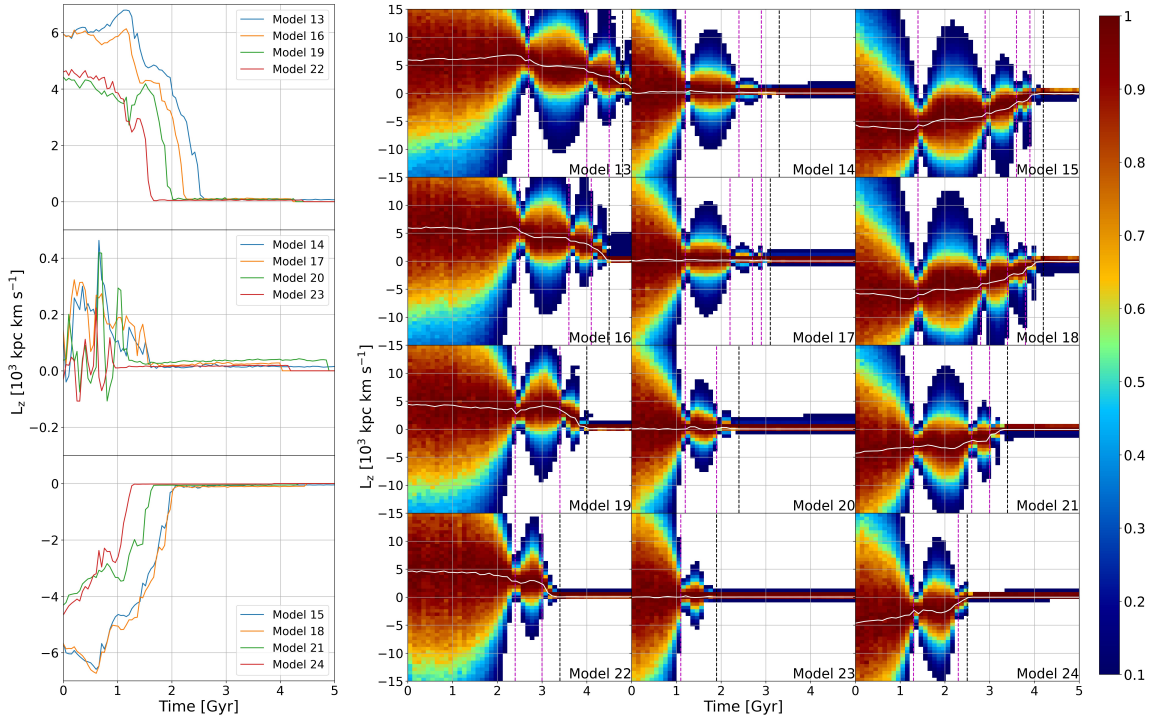
Figure 3.6: *Left column:* evolution of the mean angular momentum in all models, comparing the effects of increasing gas fraction on the mean L_z. Prograde, radial and retrograde simulations are shown from top to bottom. *Right:* evolution of the angular momentum distribution for all stars in the GSE-like satellite. At each output time step the distributions are normalized by the maximum value. The magenta dashed lines mark pericenters of the orbit, the black dashed lines t_{merg}, and the white curve the mean L_z. After the merger, the L_z distribution of GSE stars is compressed into a radial component across all models.

lations. In the left panels, the mean trends are shown to compare the evolution in the case of prograde (top), radial (middle) and retrograde (bottom) mergers. One can see that, soon after the first pericenteric passage, the absolute values of the mean angular momenta rapidly decrease and reach $L_z \approx 0$, implying a lack of net rotation of the merger debris independently of the initial orbital parameters. In the radial merger simulations (left of Fig. 3.6, middle panel), we see that the merger debris initially gains some rotation from the Milky Way disk, but its absolute values are very small and the angular momentum dissipates shortly.

We also notice the influence of gas on the mean L_z. Blue curves represent models with $M_{\mathrm{gas}}^{\mathrm{GSE}}/M_{\mathrm{gas}}^{\mathrm{MW}} = 0$, with subsequent curves respectively illustrating the change in the L_z distribution with increasing gas fraction. The gas-rich models of the GSE-like progenitor are radialised faster than for the gasless case, which is reflective of previously discussed merger time-scales (see Fig. 3.3).
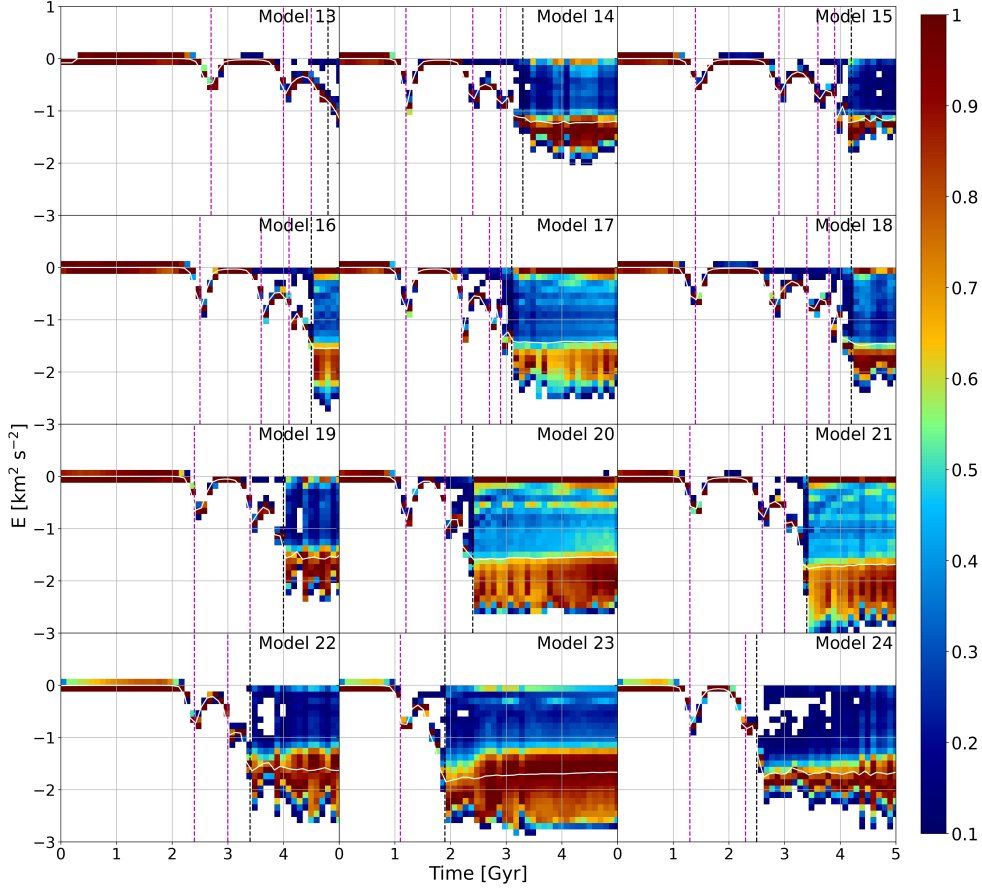
Figure 3.7: Similar to Fig. 3.6, showing the evolution of the total energy distribution of GSE stars in the Milky Way potential over time. We illustrate the enhanced binding of GSE progenitor to the Milky Way during pericentric passages. Significant amounts of scatter in the merger-debris energy distribution is shown after completion of the merger.

Another interesting result, seen in the right panels of Fig. 3.6, concerns the evolution of the angular momentum distribution. One can see that at the very early times, the L_z has a very broad distribution, but once the GSE-progenitor approaches the Milky Way, the angular momentum distribution shrinks. Then, close to the next pericenter, the distribution broadens again in a 'bottleneck'-like feature. This pattern in the L_z distribution is repeated several times until the merger is completed.

This process, although intriguing at first, is very easily interpreted. Since the angular momentum is the product of the positions and velocities (see Equ. 2.5), if we assume a constant velocity (distribution) once the satellite galaxy is moving towards the Milky Way center, its angular momentum distribution changes. Therefore, the assumption regarding the conservation of the angular momentum of the merger debris is not very precise, because the L_z changes as a result of at least three fac-

tors: generally-speaking, i) angular momentum exchange with the host galaxy, during which the satellite galaxy can gain some rotation; ii) dissipation of the angular momentum, which is more rapid in case of gas-rich simulations; iii) "by definition" even if the velocity distribution of an accreting system is rigid (no dissipation or angular momentum exchange), once the dwarf galaxy spirals in towards the center of a more massive one.

In line with the L_z analysis, we next test how much we can rely on the total energy distribution while studying the structure and evolution of the merger debris. Similarly to Fig. 3.6, we present the evolution of the total energy distribution of the stellar content of the GSE-progenitors for all the high-resolution models in Fig. 3.7. Not surprisingly, the total energy of the dwarf galaxy also does not remain unchanged. The fact that the galaxies are being accreted and their orbits decay in time already suggest that the total energy should also dissipate. This is clearly seen in Fig. 3.7, where the total energy oscillates over time starting from the very first pericenteric passage. Once the merger is completed, we observe the largest scatter in the total energy distribution, of which the bulk corresponds to the minimum energy inside the innermost parts of the Milky Way.

The effect of the gas is also quite prominent in Fig. 3.7, where the amount of gas in the system increases from the top (purely collisionless simulations) to bottom (gas-rich MW and GSE -progenitors) rows. Once gas is taken into account, the merger debris penetrates close to the minimum of the potential, where the total energy is the smallest. Therefore, the energy dissipation in the ISM is a very important factor in shaping the energy distribution of the accreted merger debris, which we discuss in details in the following Sections.

3.3 Phase-space structure of the merger debris

In this section, we take a look at the structure of the merger debris in several phase-space coordinates, which are useful in putting our models in the context on the GSE debris in the Milky Way. We have already demonstrated that both total energy and angular momentum of the merger debris evolve in time, especially during the latest stages of the merger, thus making it harder to identify physical properties of its galaxy-progenitor. However, it is worth exploring whether some of the information about the accretion event is imprinted in the stellar halo of the main galaxy after the merger is completed.

3.3.1 Present-day structure of the merger debris

First, we show the structure of the energy-angular momentum space across all of our simulations after the merger event. In Fig. 3.8, we present the stellar density distribution in $E - L_z$ coordinates for the pre-existing stars of the GSE-progenitor (left) and all stars formed during the simulations and associated with this system (right).
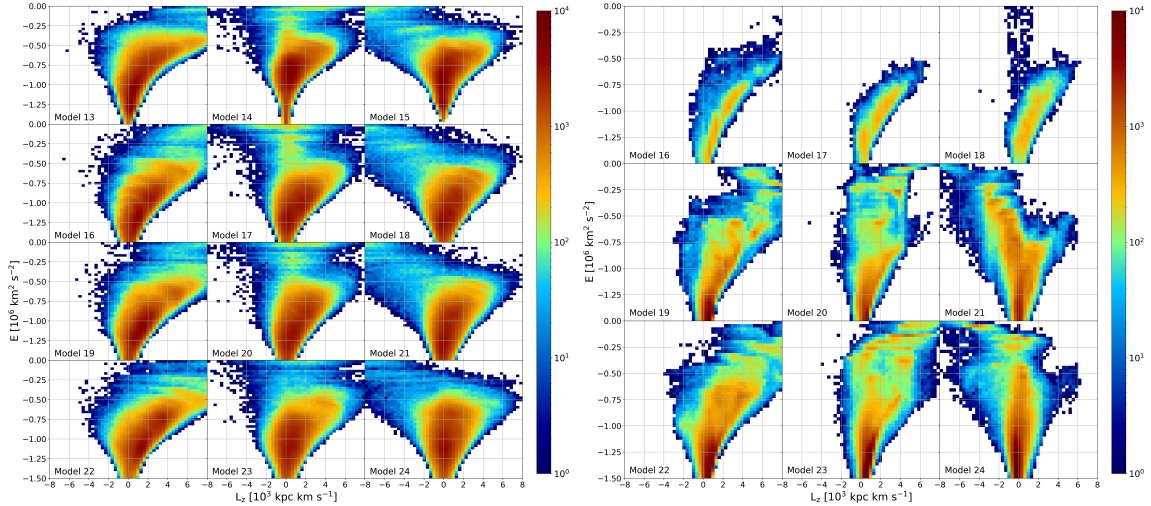
Figure 3.8: Comparison of the distribution of pre-existing (*left*) and newborn (*right*) stars in the $E - L_z$ phase space after 5 Gyr. In both cases, the general trend in the $E - L_z$ distribution is characterised by the orbit of GSE. In the right panel, Models 13-15 are excluded due to their lack of gas content and the consequent absence of star formation. Star forming content in models 16-18 is exclusive to the Milky Way due to the absence of gas in the GSE progenitor, although the new stellar population shows a clear radialised component in Model 18.

Note that gasless models are removed from the right panel as they do not exhibit star formation.

Due to the simple nature of our spatial selection in associating newborn stars to GSE (see details in Section. 2.2.4), some of the stars formed at the very last stages of evolution can be associated to the GSE-progenitor (in particular, notice the contamination in Model 18 by a radial population) although such models do not initially contain gas inside the dwarf satellite. We know these stars belong to GSE due to the radialisation of the angular momentum distribution of the satellite post-merger seen in Fig. 3.6.

As we have seen in the evolution of both E and L_z (Figs. 3.6, 3.7), the final distributions are very broad, covering almost the entire region of the diagrams. However, the phase-space structure of the GSE debris is not featureless. Even the distribution of pre-existing stars (left of Fig. 3.8) show a number of substructures and small-scale overdensities which are the most prominent at the highest energies (least bound component). We must emphasize that our models include a single merger event, implying that all these small substructures are linked to the single progenitor. Therefore, it is highly likely that some of the $E - L_z$ overdensities discussed in the literature can, in fact, represent the same progenitor galaxy despite having very different kinematics and occupying different regions of $E - L_z$ space.

The stars formed during the evolution of the system, from the ISM of the GSE-
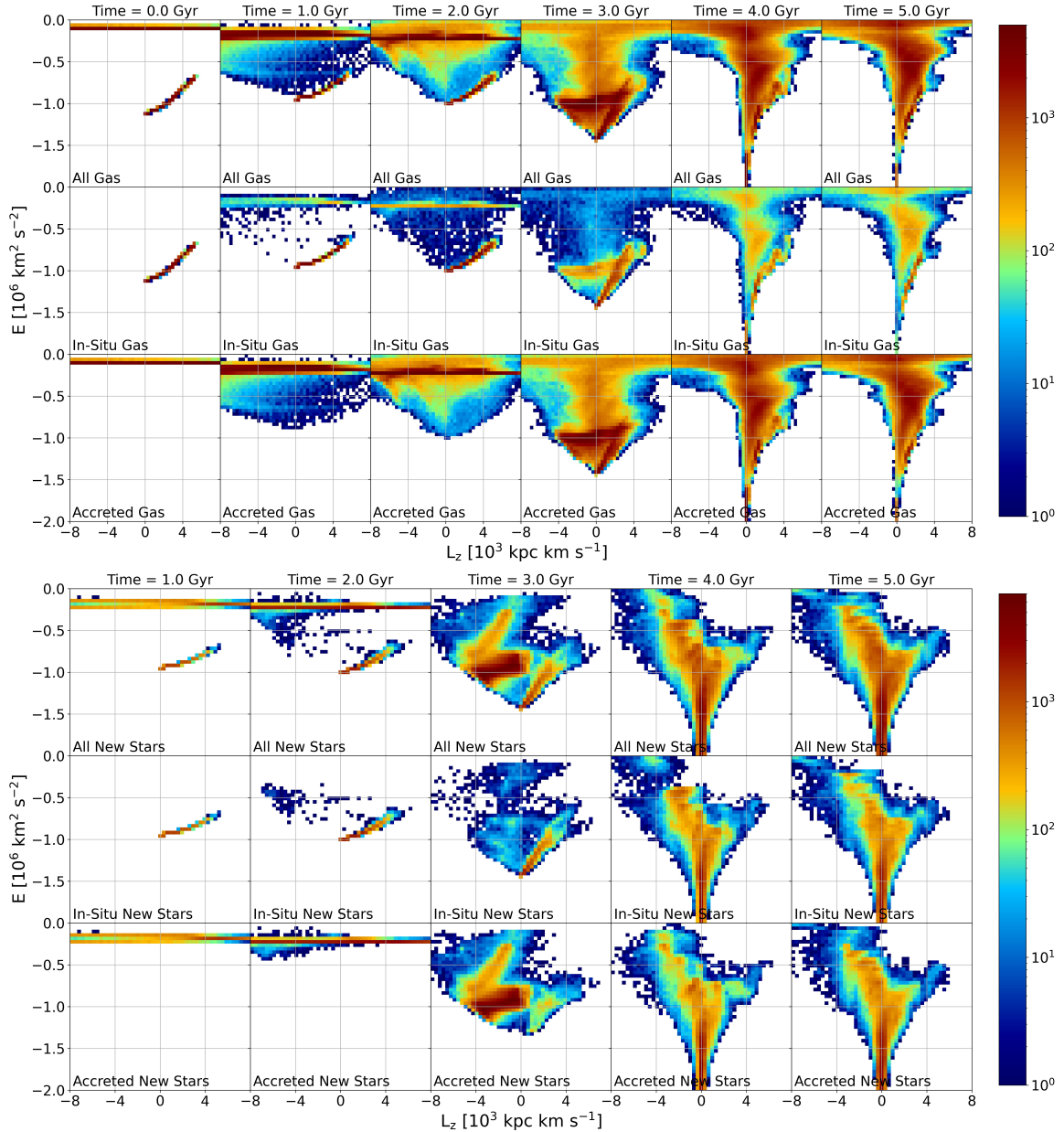
Figure 3.9: Evolution across 5 Gyr of the distribution of gas (*top*) and new stars (*bottom*) for Model 21 in E-L_z phase space. In the top row of each panel, Milky Way and GSE particles are plotted together. They are then plotted separately according to their host galaxy, respectively the Milky Way ("in-situ") and GSE ("accreted"), in subsequent rows. The accretion of the GSE progenitor results in the radialisation of the in-situ population, with a retrograde 'tail' in the final angular momentum distribution of the merger debris. This is characterised by the orbit of the accreted satellite.

progenitor, also show a number of features, which are however not identical to the ones observed for pre-existing stars. Note another interesting behaviour of newly formed stars, which we find tend to have low energies (tightly bound to the host galaxy). Most of the young stars are expected to form in the center of the GSE-progenitor and, being more bound to its core and dragged by the dynamical friction, they tend to move closer to the center of the Milky Way galaxy. Therefore, we already have some clues about the GSE-progenitor structure from the analysis of the $E - L_z$ space.

Once we compare different simulations, we clearly see some similarities and some diversities amongst the merger debris. Generally-speaking, all the mergers result in a dominantly radial component, with no net rotation, around $L_z \approx 0$. However, the prograde mergers (left columns in each set of panels of Fig. 3.8) remain prograde in the upper parts of the $E - L_z$ distribution. Interestingly, the radial mergers also tend to show some net rotation (as already discussed above) at high-energies. The most complex is the structure of the retrograde mergers, which still show some retrograde behaviour in the least bound upper parts of the $E - L_z$ and some prograde rotation (but smaller in comparison to radial and prograde mergers). Interestingly, our retrograde models (especially Model 21 and Model 24) suggest that the Sequoia substructure [69, 87, 86] can be easily associated with the GSE-progenitor. In this case, one can even also expect some differences in the chemical composition due to different behaviour of young and old stars. We discuss this possibility in the following sections.

In an attempt to disentangle the complex structure in the $E - L_z$ distribution of newborn stars for gas-rich, retrograde merger models, we plot the evolution of gas and new stars in Model 21 over 5 Gyr in $E - L_z$ phase-space in Fig. 3.9. The boundary condition used to differentiate new stars born in the GSE-like galaxy and those born in-situ is discussed in Sect. 2.2.2. We see that the the nurseries for star formation correspond to the dense regions of gas in the $E - L_z$ distribution. The rapid evolution of the gas distribution ultimately leads to the substructure in the final $E - L_z$ plots shown in Fig. 3.8.

We indeed observe in-situ star formation with distinctly prograde L_z after 1 Gyr, corresponding to star formation within the disk of the Milky Way, as well as new stars formed in GSE with large scatter in L_z, which is consistent with its L_z distribution at that time (recall Fig. 3.6).

The most interesting substructure is revealed at 3 Gyr, which coincides withe the time of the final pericentric passage of the GSE orbit for Model 21. Stars formed in the Milky Way disk have been largely radialised and the spread in L_z of in-situ new stars has started to scatter, most likely as a result of perturbations in the Milky Way disk caused by the tidal interactions with GSE. Looking at accreted new stars, we see a slight population with similar L_z to the Milky Way disk, suggesting the start of some mixing between the two galaxies.

The distribution of new stars is split into a slight prograde branch and a largely retrograde tail after the merger. From the independent distributions of in-situ and
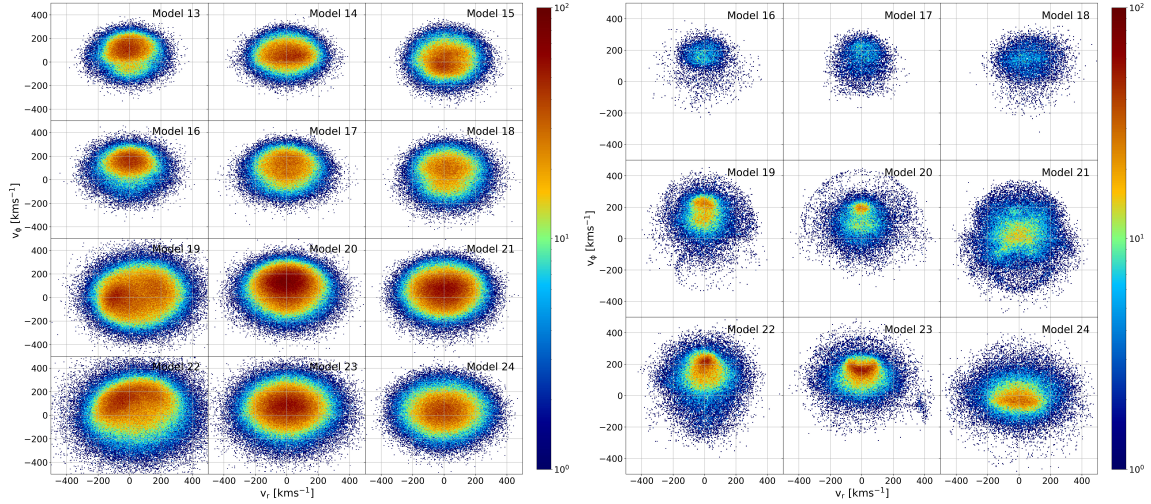
Figure 3.10: Structure of the GSE-like merger debris in the $V_r - V_\phi$ (galactocentric cylindrical radial and azimuthal velocity) kinematic space for pre-existing GSE-progenitor stars (*left*) and stars formed during the simulations (*right*). The density distributions are based on radial selections of $5 - 15$ kpc. The presented phase-space represents the original one, used to discover the bulk of the GSE stars using SDSS and LAMOST datasets (see Fig.2 in Appendix A [1]) In each set of panels, prograde, radial and retrograde mergers are shown in left, middle and right columns, respectively.

accreted populations at earlier times, we can deduce that the prograde branch originates from star formation within the Milky Way and that the retrograde tail is dictated by stars formed within the GSE-progenitor. This once again proves that a single gas-rich accretion event can self-consistently reproduce the retrograde Sequoia population, which could belong to stars formed in the outer parts of the retrograde GSE-progenitor stripped early on.

Moving on from the $E - L_z$ analysis, we also investigate the MW-GSE merger debris in velocity phase-space. In Figure 3.10 we show the stellar density distribution in a purely kinematic space (galactocentric radial - azimuthal velocity, $V_R - V_\phi$) based on the stars located in the galactocentric radial range of $5 - 15$ kpc. In the left set of panels, we show the density of the pre-existing stars of the GSE-progenitor, which reveal almost featureless blob-like distributions. They suggest that the merger debris inherited some properties of the orbit of the accreted galaxy. In particular, we see some net rotation in prograde and radial mergers (left and center columns). However, the rate of rotation is rather small and decreases with increasing mass of gas in the system, highlighting the importance of the collisional component in shaping the merger debris structure.

Once we look at the behaviour of newly formed stars, we can clearly see some differences compared to the pre-existing stars. A striking feature here is the appearance
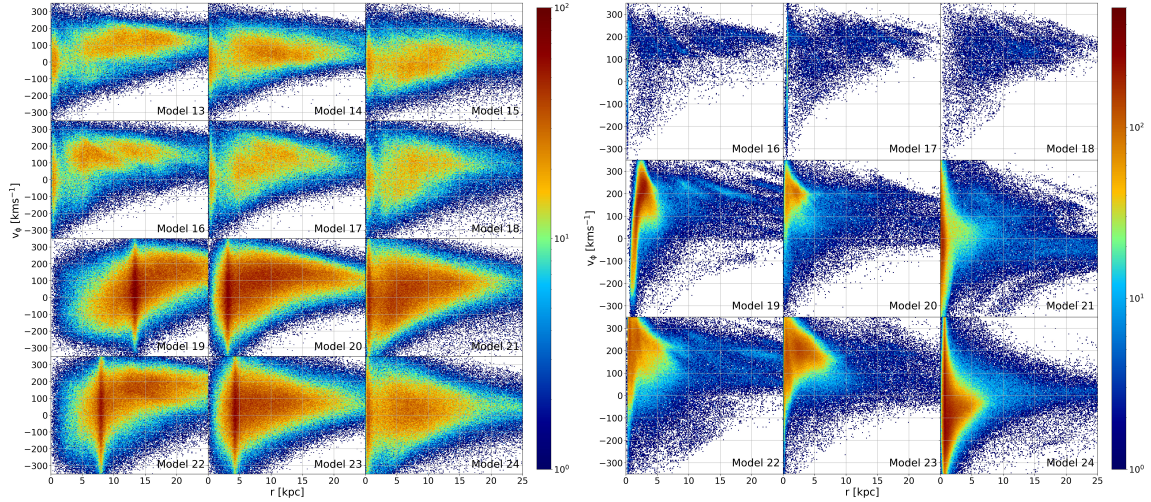
Figure 3.11: Similar to Fig. 3.10, but for the $R - V_\phi$ (galactocentric distance - azimuthal velocity) phase-space without the radial selection.

of the Sausage-like features in the retrograde simulations (rightmost columns in the right set of panels of Fig. 3.10) which are not detected neither in prograde nor in the radial merger simulations. We also note some small substructures around the bulk of stars representing still unmixed tails of the merger debris, which are similar to the ones recently discovered using Gaia DR3 datasets [93].

A notable difference between the pre-existing and newly formed stars suggests that the Sausage merger debris found in the Gaia datasets may also represent the stars which are formed just before the merger, thus biasing the properties of the accreted stellar populations, where the oldest stars of the GSE merger are distributed more homogeneously in the phase-space and, thus, can not be associated with any phase-space features. Therefore, we suggest that in order to constrain better the parameters of the GSE accretion event in the Milky Way, it is also worth exploring the distributions of background stars in various phase-spaces, in particular $V_R - V_\phi$ kinematic space.

Since in Fig. 3.10 we presented the kinematic space based on the radial selection, it is important to analyze the observed behaviour as a function of galactocentric distance. In Fig. 3.11, we show the merger debris density distribution in $R - V_\phi$ phase-space. Here, for pre-existing stars (left set of panels) one can see a very broad distribution which however very strongly changes once we include a substantial amount of gas (from top with gasless simulations to bottom with gas-rich models). We note that in the gasless simulations, one still can notice some overdensities related to the unmixed state of the GSE-like merger, while in the gas-rich models, all the features are smeared out. This suggests that gas plays a crucial role in shaping the present-day structure of accreted systems.

At the same time, newly formed stars again reveal a number of substructures

in a form of diagonal ridges. Note another important feature of the stellar density structures in the $R - V_\phi$ plane in the form of a tail around $V_\phi = 0$, reflecting the radial dependence of the merger debris structure. Therefore, the coming large-scale surveys, especially those targeting the innermost regions of the Milky Way disk (4MOST and MOONS) will play an important role in constraining the properties of the GSE merger in the Milky Way.

3.3.2 Imprint of the progenitor structure and merger process in phase-space

We pursue our analysis in $E - L_z$ phase-space, this time investigating the merger properties discussed in Sect. 3.1 are imprinted therein. In this way, we are able to explore the effect that the infall of the GSE-progenitor had on the kinematics of its stellar mass.

In Fig. 3.12, we illustrate how the escape time distribution for Model 21 is imprinted in $E - Lz$ phase space. We interestingly reveal some slight amounts of substructure within the kinematic space; particles with $t_p^1 < t_{esc} < t_p^2$ form a characteristic retrograde 'blob' when projected in $E - L_z$ phase-space, as well as a highly retrograde, weakly bound 'dash'. A similar retrograde feature, yet more pronounced, is found for stars escaped between the following pericentric passages, ie with $t_p^2 < t_{esc} < t_p^3$. This again goes to show the retrograde features of star populations accreted early on, which can undoubtedly be linked to Sequoia.

We also show in Fig. 3.12 that the fraction of escaped stellar mass is in fact significantly lower than the total stellar content of the GSE-like progenitor, which is a result of the tight gravitational binding of stars in the GSE bulge. This stands out more in the bottom-left-most panel, in which we see that the fraction of never escaped stellar mass to total stellar mass is ≈ 1 for the most part, with the only exceptions being slight amounts of substructure in the retrograde tail mentioned above and some scatter in the prograde component. We are therefore able to trace some contributions of escaped particles to the final $E - L_z$ distribution of GSE after the merger, although the fraction of escaped to contained stars is rather small.

In order to understand the fate of the initial structure of the GSE-progenitor, we also investigate how GSE stars are distributed in $E - L_z$ phase space as a function of R_0^{GSE} in the final merger debris. This plot is shown in Fig. 3.13. We prove that stars initially found close to the center of GSE correspond to those found on radial orbits, most tightly bound to the Milky Way after the merger. As previously discussed, the center of the GSE-like satellite is tightly bound within itself and doesn't dissociate during the merger event. Hence, its stars are not dispersed into the Milky Way during the orbit and the GSE center merges with that of the Milky Way. We note that with increasing gas fraction, the density of stars with low R_0^{GSE} and radial orbital characteristics is more tightly bound.

Stars located further out at the start of the simulation are those that give the
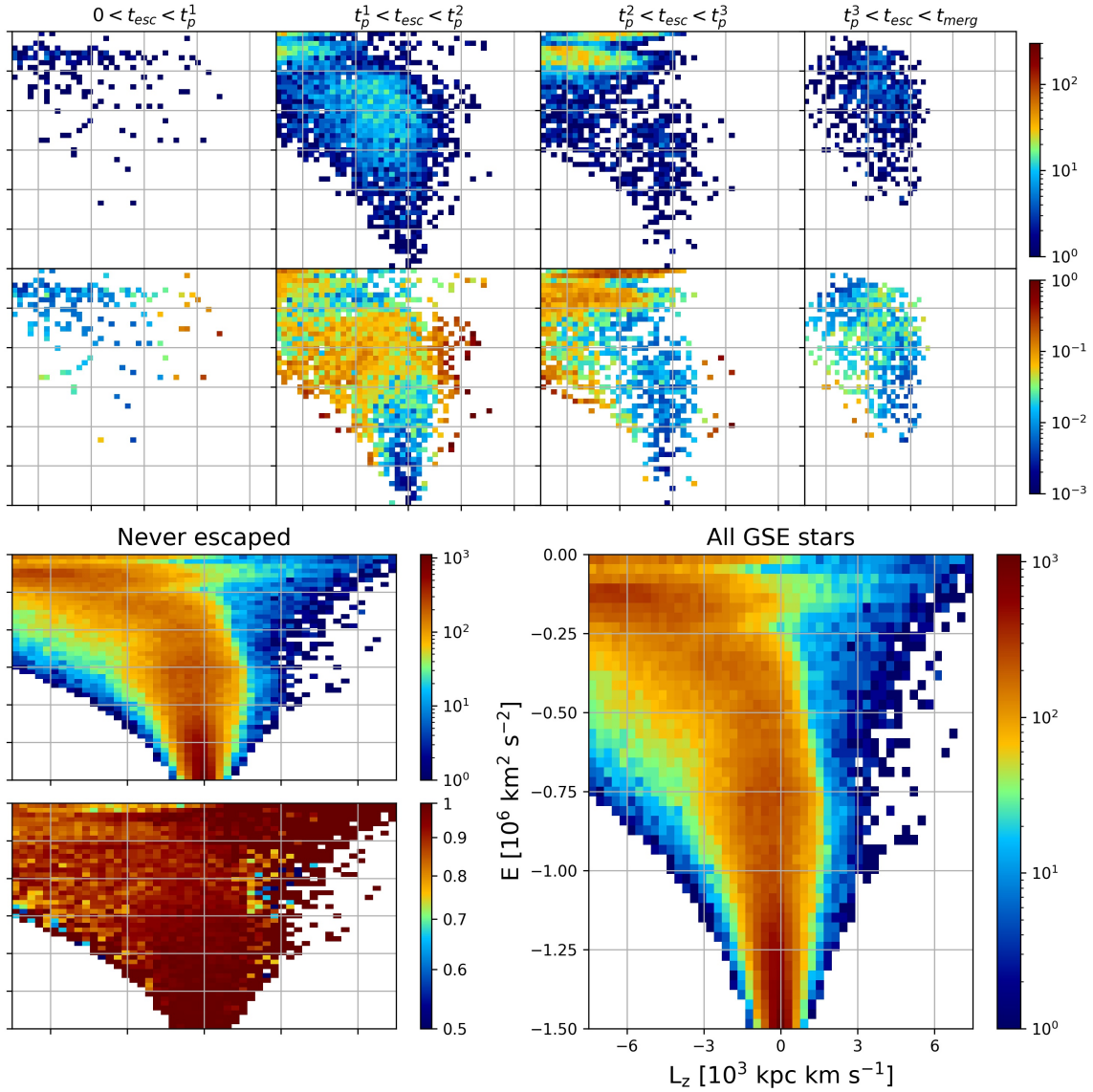
Figure 3.12: Projection of the escape times of GSE stars in $E - L_z$ phase-space for Model 21 after 5 Gyr. *Top*: Compartmentalisation of stars into bins according to their escape times, encapsulated between the times of the pericentric passages. On the upper row, the number density of stars escaped is shown. On the lower row, we show the fraction of the total GSE stellar mass that this represents. The majority of stars that escape GSE are stripped from the dwarf galaxy during the middle stages of the merger, although they represents a small fraction of its total stellar mass. *Bottom*: On the left, the $E - L_z$ distribution of never-escaped GSE stars. The majority of stars contained in GSE remain within its bulge throughout the accretion event, thus never escaping the accreted galaxy. On the right, the $E - L_z$ distribution of all (escaped and pre-existing) GSE stars are plotted. All plots have identical axes to this panel.
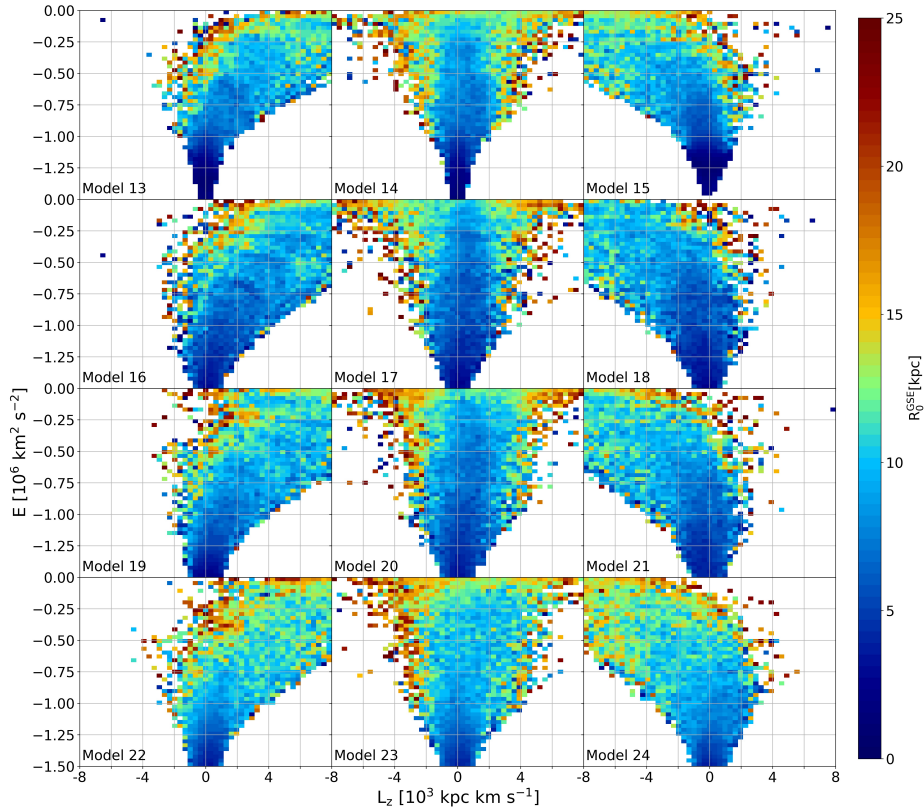
Figure 3.13: $E - L_z$ distribution of the final GSE merger debris after 5 Gyr coloured by mean initial radius from the GSE center, R_0^{GSE}. Stars located near the center of the GSE satellite at the start of the simulations find themselves more bound to the Milky Way after the merger, with an angular momentum tail once again reflecting the orbital characteristics of the GSE progenitor.

merger debris their characteristic prograde or retrograde 'tails' in their distributions. With the MW disk showing prograde characteristics in $E - L_z$ phase-space [1], this implies that in the case of retrograde models, namely Model 21, the accreted stars initially found in the outskirts of GSE are the cause of the radialised debris within the MW after the merger (see Section 2.2.2, Fig. 2.2).

3.4 Star Formation Histories

Thanks to the tremendous amount of spectroscopic information about the MW stellar populations, we are able to explore different stages of the MW formation and evolution. Formation of the chemically-defined thick (so-called high-α sequence) disk started soon after the Big Bang [94, 95, 96]. The thin disk (or low-α sequence) started forming at around $8 - 10$ Gyr ago [97, 98, 99]. The end of the first process and the
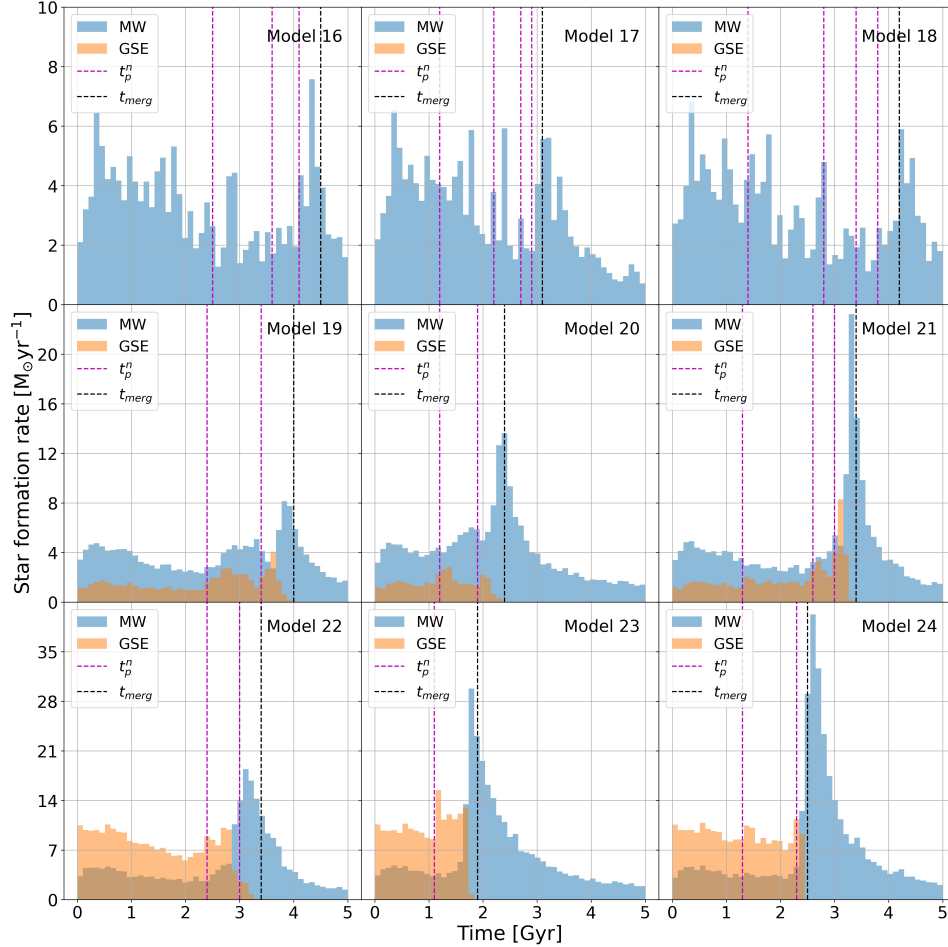
Figure 3.14: Comparison of SFHs across all MW-GSE merger models. In blue, the SFH of the MW. In orange, the SFH in the GSE. Major star formation bursts are observed at the time of the merger (black dashed line), with minor peaks in star formation between pericentric passages of the GSE orbit (magenta dashed lines).

beginning of the second one coincidentally connect to each other at the time of the GSE merger $(8-11$ Gyr ago).

Therefore, it is crucial to understand how much the star formation rate of the Milky Way has evolved at that time. Using our simulations, we explore the SFHs of the Milky Way and GSE during the merger event. With larger amounts of gas available, we naturally expect a considerable increase in star formation across models with increasing gas fraction. The SFHs for our merger models are illustrated in Fig. 3.14, where we plot the SFR as a function of time and show that this is indeed the case.

For the simulations with no gas inside the -GSE (top row), we observe a lot of scatter in the SFR with some peaks correlating the pericentric passages of the GSE-

progenitor. However, amongst the scatter, the general trend is a slight decrease in star formation with a substantial increase of the SFR at the time merger. We see that the Milky Way SFR is affected by a gasless GSE progenitor, although its effect is very subtle. Thus we conclude that even a pure perturbation from the GSE-like merger is enough to enhance the star formation rate via contraction of the gas (see also [100]).

However, we notice more prominent bursts in the SFRs at the time of the merger for gas-rich GSE models (middle and bottom rows of Fig. 3.14), suggesting the existence of a population of younger stars in the merged system. As the galaxies merge, large amounts of gas and dust are funnelled towards the centre of the Milky Way, creating a dense, high-pressure environment. This, combined with the compression of gas by gravitational forces [101], can lead to the rapid formation of new stars, which we observe in our model. We nevertheless note an earlier burst of star formation in Model 22. The tidal interactions between the Milky Way and GSE near the pericenters of the orbit have an effect on the SFHs, with prominent bursts in star formation within GSE following its pericentric passages seen in Models 20, 21, 23 and 24, confirming recent results presented in [102]. Within the Milky Way, we rather notice a gradual buildup in the SFR during the merger timescale. Therefore, our models do not suggest a correlation between the Milky Way star formation rate and the close passages of massive satellites, except for the very latest stages of the merger.

In Fig. 3.14, we also see that the orbital properties of the GSE-like progenitor play a significant role in defining the intensity of the starburst. Interestingly, across all the simulations, the retrograde merger models exhibit the highest peak in SFR (rightmost column) at the time of the merger. For a merger on a retrograde orbit, the counter-rotating features of the GSE progenitor cancels the rotational angular momentum of the MW disk, in turn reducing the net angular momentum of the gas which is itself funnelling to the inner regions of the galaxy, thus favouring a more intense starburst. In the case of the prograde orbit, the collision of two co-rotating gas components (MW and GSE) is not so drastic and the gas contraction is therefore smaller. Hence, the observed star formation burst is also not so prominent.

In order to further explore the star formation process within the Milky Way-GSE-like merger, we calculate the star formation distance (SFD) relative to the center of the Milky Way. The plots are shown in Fig. 3.15. In the gasless GSE models (top row), we see that star formation is stable within $R_{sf} \leq 25$ kpc. Once the orbit of GSE reaches a galactocentric distance of 25 kpc at later times, a slightly increased star formation is noticeable around its path. After the merger is complete, we notice a burst in star formation near $R_{SF} \approx 0$, consistent with conclusions drawn from Fig. 3.14 for these models.

This burst in star formation at $R_{SF} \approx 0$ after the time of the merger is flagrant in subsequent, gas-rich GSE models. These illustrate the orbit of GSE through the birth of new stars during its accretion. Star formation is strongest in the GSE-like progenitor compared to the Milky Way due to a larger relative gas fraction and smaller
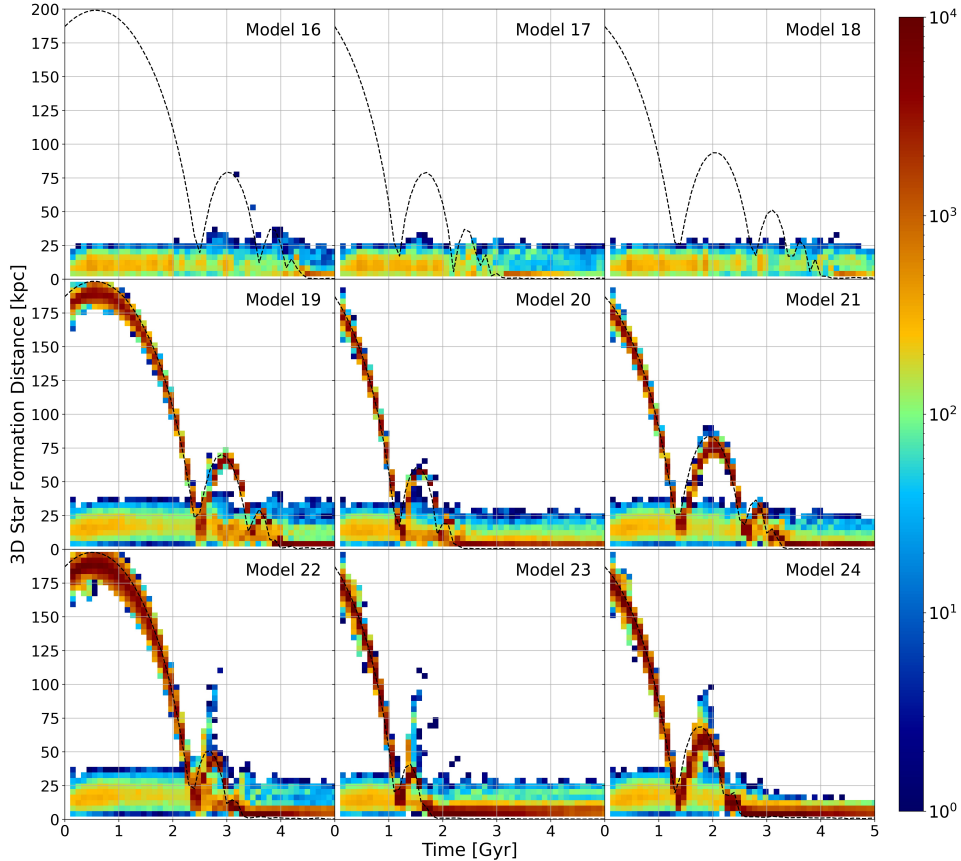
Figure 3.15: Star formation histories of simulated galaxies, as shown by 2D histograms of formation distance versus formation time, for new star particles inside the GSE-progenitor and the Milky Way. Star formation in the Milky Way is comprised within the Milky Way disk. The SFR of stars born within the infalling GSE satellite during the merger event trace the orbital decay of the dwarf galaxy, shown as a black dashed line (see Fig. 3.2).

size of the GSE-progenitor galaxy. We observe star formation in the Milky Way at slightly larger distances than in gasless-GSE models, perhaps due to the accretion of gas to the outskirts of the Galaxy early on.

The Milky Way star formation occurs within a smooth radial band, which is densest between $10 \leq R_{SF} \leq 25$ kpc. We deduce that Milky Way star formation is most dense within its disk, with less new stars being born in the bulge ($R_{SF} < 10$kpc) and in the stellar halo($R_{SF} > 25$kpc). This band is perturbed at the pericenters of GSE, where we find bursts of star formation in the entirety of the Milky Way. We indeed notice the dense population of new stars dipping to lower galactocentric distances than the mean position of the satellite during pericentric passages. In the most gas-rich models, we also see bursts of star formation at large radial distances.

The peaks in SFD between pericentric passages may be a result of the scatter of gas during the merger event.

To summarize, we showed that the GSE-like merger enhances the star formation rate in the MW-like disk. The effect is small, but not negligible even in models where the GSE-progenitor galaxy does not contain any gas. Intuitively, the characteristics of the SFRs (namely peaks corresponding to starbursts) gradually become more prominent with increasing gas fraction in the accreted galaxy. We find that the SFR is most enhanced in the case of the retrograde gas-rich merger, with further enhancement inside the GSE-progenitor during its close pericentric passages that could in turn affect its chemical enrichment rate.

Chapter 4

Project summary

Galactic research has entered a thrilling epoch. Our knowledge about Galactic stellar populations, which was mostly confined to stars in the solar vicinity up until just a few years ago, is rapidly extending to larger and larger regions of the disk, bulge and outer halo of the Milky Way. The Gaia (ESA) satellite mission is giving us parallaxes, proper motions, and line-of-sight velocities with unprecedented precision and, thus, once combined with the spectroscopic information from ground-based surveys, allows us to quantify the complex dynamical processes driving the evolution of the Milky Way. Therefore, it is now time to understand better the complexity of underlying physical processes shaping Galactic stellar populations.

Detection of the stellar debris from an ancient, massive accretion is likely the biggest and even paradigm-shifting discovery of recent years in Galactic astronomy. In light of the discovery of Gaia-Sausage-Enceladus, in order to build a coherent picture of the formation of the Milky Way, we now need to understand not only how its main stellar components (disk, bulge) evolved, but also the properties of accreted dwarf galaxies which are now buried in the Galactic halo and the bulge regions. As well as this, the way in which the structure and kinematics of these ancient objects are imprinted in the present-day kinematic-space and chemical abundance relations of the Milky Way stellar populations must be better understood.

The backbone of this theoretical project is a set of hydrodynamical simulations of galaxy mergers tailored to understand the origin of several features of the GSE-merger debris. This project aimed to answer some of the simplest yet still unanswered questions: What are the characteristics of the stellar component accreted during a single massive galaxy merger? How are these populations shaped over time depending on the orbit and intrinsic structure of the galaxy-progenitor?

The main scientific results of our work are summarized as follows.

1. We found that the merger time scale and a number of pericentric passages prior to coalescence of the GSE-like progenitor significantly depend on the direction of the orbit and the relative gas fraction of the Milky Way and accreted galaxy (see

Fig. 3.2). Radial infall happens on the shortest time scale compared to prograde and retrograde ones. The merger time scale reduces even more if both the Milky Way and the GSE galaxies were gas-rich at the time of accretion. Our models show that the shortest accretion time scale is about 2 Gyr (Model 23: Massive gas content, radial orbit), and the longest is about 5 Gyr (Model 13: Gasless, prograde orbit). These numbers are the essential input for galactic chemical evolution models of the GSE-progenitor because they put constraints on the time scale of the GSE proto-galaxy enrichment.

2. We demonstrated that the widely-used assumptions regarding the coherence of the merger debris in the energy-angular momentum space are not applicable to a MW-GSE-like massive merger. We found that both the total energy and angular momentum change significantly starting from the first pericentric passage until the full coalescence of the galaxies (MW and GSE-progenitor), as a result of dynamical friction and collisional effects of the ISM (see Figs. 3.6, 3.7). Therefore, most of the information regarding the progenitor galaxy was lost. Nevertheless, some information can still be recovered from the $E - L_z$ distribution of the merger debris. We showed that the merger remnant from a single GSE-like event is not clustered in $E - L_z$ phase-space and is spread out over a large area in these coordinates. However, at the same time, the $E - L_z$ distributions are not featureless, as a single merger remnant often contributes to a few overdensities. In particular, we found that the retrograde mergers with a substantial amount of gas best reproduce the observed kinematic $V_r - V_{phi}$ structure (see Figs. 3.10). At the same time, only these models can simultaneously explain the Sequoia substructure, which, according to our models, could belong to the outer parts of the retrograde GSE-progenitor stripped early on and, thus, preserving some retrograde motion (see Figs. 3.8,3.9,3.12).

3. Our models predict that the internal structure of the GSE-progenitor is imprinted in the structure of the stellar merger debris. If the GSE-like proto-galaxies had radial abundance gradients, then the accreted stellar debris are also expected to reveal the abundance gradients in the $E - L_z$ plane. The inner parts of accreted galaxies contribute mainly to the central regions of the Milky Way galaxy with the lowest energies; the upper parts of the $E - L_z$ space is mainly populated by the stars formed at the outskirts of accreted systems (see Fig. 3.13). Therefore, the search for the abundance variations in the $E - L_z$ space with coming spectroscopic surveys (4MOST, MOONS) will shed light on the characteristics of the accreted dwarf galaxies.

4. We showed that the accretion of the GSE-like galaxy inevitably results in the burst of the star formation inside the Milky Way. From our models, we show that during the merger the Milky Way SFR rapidly increases by a factor of ≈ 10, which is illustrated in our gas-rich simulations of the retrograde merger.

Such models best reproduce the phase-space structure of the merger debris (see Fig. 3.14). Therefore, even if the star formation efficiency in the Milky Way at the time of the GSE-infall was lower compared to our models, the amount of gas delivered (and still remained in the gas-rich Milky Way) by the GSE-progenitor should be enough to sustain the star formation rate in the MW over the next epoch of its disk formation.

The findings we make from our N-body/hydrodynamical simulations set up the scene for new, future theoretical models. The next step towards the correct reconstruction of the merger tree of the Milky Way will require better constraints on properties (chemical abundance trends, mass spectrum, rate of rotation, DM and gas content) of dwarf galaxies which did not survive until present but have been accreted at the early phases of the Milky Way formation.

References

[1] V. Belokurov et al., "Co-formation of the disc and the stellar halo," *MNRAS*, vol. 478, no. 1, pp. 611–619, Jul. 2018.

[2] C. J. Conselice et al., "The Evolution of Galaxy Number Density at z ¡ 8 and Its Implications," *ApJ*, vol. 830, no. 2, p. 83, Oct. 2016.

[3] R. B. Tully et al., "The Laniakea supercluster of galaxies," *Nature*, vol. 513, no. 7516, pp. 71–73, Sep. 2014.

[4] F. Zwicky, "On the Masses of Nebulae and of Clusters of Nebulae," *ApJ*, vol. 86, p. 217, Oct. 1937.

[5] V. C. Rubin, J. Ford, W. K., and N. Thonnard, "Rotational properties of 21 SC galaxies with a large range of luminosities and radii, from NGC 4605 (R=4kpc) to UGC 2885 (R=122kpc)." *ApJ*, vol. 238, pp. 471–487, Jun. 1980.

[6] Planck Collaboration, "Planck 2013 results. XVI. Cosmological parameters," *A&A*, vol. 571, p. A16, Nov. 2014.

[7] V. Springel, "The cosmological simulation code GADGET-2," *MNRAS*, vol. 364, no. 4, pp. 1105–1134, Dec. 2005.

[8] V. Springel et al., "Simulations of the formation, evolution and clustering of galaxies and quasars," *Nature*, vol. 435, no. 7042, pp. 629–636, Jun. 2005.

[9] D. Kereš et al., "How do galaxies get their gas?" *MNRAS*, vol. 363, no. 1, pp. 2–28, Oct. 2005.

[10] J. Schaye et al., "The EAGLE project: simulating the evolution and assembly of galaxies and their environments," *MNRAS*, vol. 446, no. 1, pp. 521–554, Jan. 2015.

[11] S. D. M. White and C. S. Frenk, "Galaxy Formation through Hierarchical Clustering," *ApJ*, vol. 379, p. 52, Sep. 1991.

[12] C. Scannapieco et al., "The Milky Way and Andromeda galaxies in a constrained hydrodynamical simulation: morphological evolution," *A&A*, vol. 577, p. A3, May 2015.

[13] C. J. Grillmair and O. Dionatos, "Detection of a 63° Cold Stellar Stream in the Sloan Digital Sky Survey," *ApJ*, vol. 643, no. 1, pp. L17–L20, May 2006.

[14] D. Martínez-Delgado et al., "Stellar Tidal Streams in Spiral Galaxies of the Local Volume: A Pilot Survey with Modest Aperture Telescopes," *AJ*, vol. 140, no. 4, pp. 962–967, Oct. 2010.

[15] A. M. Atkinson, R. G. Abraham, and A. M. N. Ferguson, "Faint Tidal Features in Galaxies within the Canada-France-Hawaii Telescope Legacy Survey Wide Fields," *ApJ*, vol. 765, no. 1, p. 28, Mar. 2013.

[16] P.-A. Duc et al., "The ATLAS^{3D} project - XXIX. The new look of early-type galaxies and surrounding fields disclosed by extremely deep optical images," *MNRAS*, vol. 446, no. 1, pp. 120–143, Jan. 2015.

[17] R. S. de Jong et al., "4MOST: 4-metre multi-object spectroscopic telescope," in *Ground-based and Airborne Instrumentation for Astronomy IV*, ser. Society of Photo-Optical Instrumentation Engineers (SPIE) Conference Series, vol. 8446, Sep. 2012, p. 84460T.

[18] F. van Leeuwen et al., "Gaia DR3 documentation," p. 1, Jun. 2022.

[19] H. L. Morrison, "The Local Density of Halo Giants," *AJ*, vol. 106, p. 578, Aug. 1993.

[20] J. T. Mackereth and J. Bovy, "Weighing the stellar constituents of the galactic halo with APOGEE red giant stars," *MNRAS*, vol. 492, no. 3, pp. 3631–3646, Mar. 2020.

[21] K. Freeman and J. Bland-Hawthorn, "The New Galaxy: Signatures of Its Formation," *ARA&A*, vol. 40, pp. 487–537, Jan. 2002.

[22] O. J. Eggen, D. Lynden-Bell, and A. R. Sandage, "Evidence from the motions of old stars that the Galaxy collapsed." *ApJ*, vol. 136, p. 748, Nov. 1962.

[23] A. Helmi, "The stellar halo of the Galaxy," *A&A Rev.*, vol. 15, no. 3, pp. 145–188, Jun. 2008.

[24] A. Helmi et al., "Debris streams in the solar neighbourhood as relicts from the formation of the Milky Way," *Nature*, vol. 402, no. 6757, pp. 53–55, Nov. 1999.

[25] ——, "On the Nature of the Ringlike Structure in the Outer Galactic Disk," *ApJ*, vol. 592, no. 1, pp. L25–L28, Jul. 2003.

[26] F. A. Gómez et al., "Vertical density waves in the Milky Way disc induced by the Sagittarius dwarf galaxy," *MNRAS*, vol. 429, no. 1, pp. 159–164, Feb. 2013.

[27] L. Searle and R. Zinn, "Composition of halo clusters and the formation of the galactic halo." *ApJ*, vol. 225, pp. 357–379, Oct. 1978.

[28] S. R. Majewski, J. A. Munn, and S. L. Hawley, "Absolute Proper Motions to B approximately 22.5: Large-Scale Streaming Motions and the Structure and Origin of the Galactic Halo," *ApJ*, vol. 459, p. L73, Mar. 1996.

[29] J. S. Bullock and K. V. Johnston, "Tracing Galaxy Formation with Stellar Halos. I. Methods," *ApJ*, vol. 635, no. 2, pp. 931–949, Dec. 2005.

[30] E. F. Bell et al., "The Accretion Origin of the Milky Way's Stellar Halo," *ApJ*, vol. 680, no. 1, pp. 295–311, Jun. 2008.

[31] M. G. Abadi, J. F. Navarro, and M. Steinmetz, "Stars beyond galaxies: the origin of extended luminous haloes around galaxies," *MNRAS*, vol. 365, no. 3, pp. 747–758, Jan. 2006.

[32] D. Carollo et al., "Two stellar components in the halo of the Milky Way," *Nature*, vol. 450, no. 7172, pp. 1020–1025, Dec. 2007.

[33] T. C. Beers et al., "The Case for the Dual Halo of the Milky Way," *ApJ*, vol. 746, no. 1, p. 34, Feb. 2012.

[34] R. Schönrich, M. Asplund, and L. Casagrande, "Does SEGUE/SDSS indicate a dual Galactic halo?" *ApJ*, vol. 786, no. 1, p. 7, May 2014.

[35] G. De Lucia and A. Helmi, "The Galaxy and its stellar halo: insights on their formation from a hybrid cosmological approach," *MNRAS*, vol. 391, no. 1, pp. 14–31, Nov. 2008.

[36] A. S. Font et al., "Chemical Abundance Distributions of Galactic Halos and Their Satellite Systems in a ΛCDM Universe," *ApJ*, vol. 638, no. 2, pp. 585–595, Feb. 2006.

[37] D. Carollo et al., "Carbon-enhanced Metal-poor Stars in the Inner and Outer Halo Components of the Milky Way," *ApJ*, vol. 744, no. 2, p. 195, Jan. 2012.

[38] A. Helmi, "Streams, Substructures, and the Early History of the Milky Way," *ARA&A*, vol. 58, pp. 205–256, Aug. 2020.

[39] C. W. Purcell, J. S. Bullock, and S. Kazantzidis, "Heated disc stars in the stellar halo," *MNRAS*, vol. 404, no. 4, pp. 1711–1718, Jun. 2010.

[40] Y. Qu et al., "Characteristics of thick disks formed through minor mergers: stellar excesses and scale lengths," *A&A*, vol. 530, p. A10, Jun. 2011.

[41] A. S. Font et al., "Cosmological simulations of the formation of the stellar haloes around disc galaxies," *MNRAS*, vol. 416, no. 4, pp. 2802–2820, Oct. 2011.

[42] I. G. McCarthy et al., "Global structure and kinematics of stellar haloes in cosmological hydrodynamic simulations," *MNRAS*, vol. 420, no. 3, pp. 2245–2262, Mar. 2012.

[43] K. Malhan et al., "The Global Dynamical Atlas of the Milky Way Mergers: Constraints from Gaia EDR3-based Orbits of Globular Clusters, Stellar Streams, and Satellite Galaxies," *ApJ*, vol. 926, no. 2, p. 107, Feb. 2022.

[44] C. Mateu, "galstreams: A Library of Milky Way Stellar Stream Footprints and Tracks," *arXiv e-prints*, p. arXiv:2204.10326, Apr. 2022.

[45] N. F. Martin et al., "The PAndAS Field of Streams: Stellar Structures in the Milky Way Halo toward Andromeda and Triangulum," *ApJ*, vol. 787, no. 1, p. 19, May 2014.

[46] H. Newberg et al., "The Ghost of Sagittarius and Lumps in the Halo of the Milky Way," *ApJ*, vol. 569, no. 1, pp. 245–274, Apr. 2002.

[47] S. R. Majewski et al., "A Two Micron All Sky Survey View of the Sagittarius Dwarf Galaxy. I. Morphology of the Sagittarius Core and Tidal Arms," *ApJ*, vol. 599, no. 2, pp. 1082–1115, Dec. 2003.

[48] R. A. Ibata, G. Gilmore, and M. J. Irwin, "A dwarf satellite galaxy in Sagittarius," *Nature*, vol. 370, no. 6486, pp. 194–196, Jul. 1994.

[49] D. R. Law, S. R. Majewski, and K. V. Johnston, "Evidence for a Triaxial Milky Way Dark Matter Halo from the Sagittarius Stellar Tidal Stream," *ApJ*, vol. 703, no. 1, pp. L67–L71, Sep. 2009.

[50] J. Bovy, "Detecting the Disruption of Dark-Matter Halos with Stellar Streams," *Phys. Rev. Lett.*, vol. 116, no. 12, p. 121301, Mar. 2016.

[51] A. Bonaca et al., "The Spur and the Gap in GD-1: Dynamical Evidence for a Dark Substructure in the Milky Way Halo," *ApJ*, vol. 880, no. 1, p. 38, Jul. 2019.

[52] R. Ibata et al., "Detection of Strong Epicyclic Density Spikes in the GD-1 Stellar Stream: An Absence of Evidence for the Influence of Dark Matter Subhalos?" *ApJ*, vol. 891, no. 2, p. 161, Mar. 2020.

[53] V. Belokurov et al., "The Field of Streams: Sagittarius and Its Siblings," *ApJ*, vol. 642, no. 2, pp. L137–L140, May 2006.

[54] M. Bellazzini et al., "Tracing the Sgr Stream with 2MASS. Detection of Stream stars around Outer Halo globular clusters," *A&A*, vol. 405, pp. 577–583, Jul. 2003.

[55] J. G. Cohen, "Palomar 12 as a Part of the Sagittarius Stream: The Evidence from Abundance Ratios," *AJ*, vol. 127, no. 3, pp. 1545–1554, Mar. 2004.

[56] L. Monaco et al., "Blue Horizontal-Branch Stars in the Sagittarius Dwarf Spheroidal Galaxy," *ApJ*, vol. 597, no. 1, pp. L25–L28, Nov. 2003.

[57] M. Bellazzini et al., "Detection of a population gradient in the Sagittarius stream," *A&A*, vol. 457, no. 2, pp. L21–L24, Oct. 2006.

[58] A. Miskolczi, D. J. Bomans, and R. J. Dettmar, "Tidal streams around galaxies in the SDSS DR7 archive. I. First results," *A&A*, vol. 536, p. A66, Dec. 2011.

[59] M. Odenkirchen et al., "The Extended Tails of Palomar 5: A 10° Arc of Globular Cluster Tidal Debris," *AJ*, vol. 126, no. 5, pp. 2385–2407, Nov. 2003.

[60] R. A. Ibata, K. Malhan, and N. F. Martin, "The Streams of the Gaping Abyss: A Population of Entangled Stellar Streams Surrounding the Inner Galaxy," *ApJ*, vol. 872, no. 2, p. 152, Feb. 2019.

[61] A. Helmi et al., "The merger that led to the formation of the Milky Way's inner stellar halo and thick disk," *Nature*, vol. 563, no. 7729, pp. 85–88, Oct. 2018.

[62] A. J. Deason et al., "Apocenter Pile-up: Origin of the Stellar Halo Density Break," *ApJ*, vol. 862, no. 1, p. L1, Jul. 2018.

[63] P. Di Matteo et al., "The Milky Way has no in-situ halo other than the heated thick disc. Composition of the stellar halo and age-dating the last significant merger with Gaia DR2 and APOGEE," *A&A*, vol. 632, p. A4, Dec. 2019.

[64] L. Lancaster et al., "The halo's ancient metal-rich progenitor revealed with BHB stars," *MNRAS*, vol. 486, no. 1, pp. 378–389, Jun. 2019.

[65] H. H. Koppelman, R. O. Y. Bos, and A. Helmi, "The messy merger of a large satellite and a Milky Way-like galaxy," *A&A*, vol. 642, p. L18, Oct. 2020.

[66] D. Kruijssen et al., "Kraken reveals itself - the merger history of the Milky Way reconstructed with the E-MOSAICS simulations," *MNRAS*, vol. 498, no. 2, pp. 2472–2491, Oct. 2020.

[67] R. P. Naidu et al., "Reconstructing the Last Major Merger of the Milky Way with the H3 Survey," *ApJ*, vol. 923, no. 1, p. 92, Dec. 2021.

[68] M. Haywood et al, "In Disguise or Out of Reach: First Clues about In Situ and Accreted Stars in the Stellar Halo of the Milky Way from Gaia DR2," *ApJ*, vol. 863, no. 2, p. 113, Aug. 2018.

[69] G. C. Myeong et al., "The Milky Way Halo in Action Space," *ApJ*, vol. 856, no. 2, p. L26, Apr. 2018.

[70] V. Belokurov et al., "The biggest splash," *MNRAS*, vol. 494, no. 3, pp. 3880–3898, May 2020.

[71] H. Velazquez and S. D. M. White, "Sinking satellites and the heating of galaxy discs," *MNRAS*, vol. 304, no. 2, pp. 254–270, Apr. 1999.

[72] C. W. Purcell et al., "The Sagittarius impact as an architect of spirality and outer rings in the Milky Way," *Nature*, vol. 477, no. 7364, pp. 301–303, Sep. 2011.

[73] V. Biffi et al., "On the Nature of Hydrostatic Equilibrium in Galaxy Clusters," *ApJ*, vol. 827, no. 2, p. 112, Aug. 2016.

[74] F. Matteucci, "Modelling the chemical evolution of the Milky Way," *A&A Rev.*, vol. 29, no. 1, p. 5, Dec. 2021.

[75] H. C. Plummer, "On the problem of distribution in globular star clusters," *MNRAS*, vol. 71, pp. 460–470, Mar. 1911.

[76] M. Miyamoto and R. Nagai, "Three-dimensional models for the distribution of mass in galaxies." *PASJ*, vol. 27, pp. 533–543, Jan. 1975.

[77] G. Kuzmin, "A stationary galaxy model admitting triaxial velocity distribution (in Russian)," *AJ*, vol. 33, p. 27, 1956.

[78] E. Vasiliev, "Agama reference documentation," *arXiv e-prints*, p. arXiv:1802.08255, Feb. 2018.

[79] P. F. Hopkins, "A new class of accurate, mesh-free hydrodynamic simulation methods," *MNRAS*, vol. 450, no. 1, pp. 53–110, Jun. 2015.

[80] P. F. Hopkins et al., "FIRE-2 simulations: physics versus numerics in galaxy formation," *MNRAS*, vol. 480, no. 1, pp. 800–863, Oct. 2018.

[81] V. Springel and L. Hernquist, "Cosmological smoothed particle hydrodynamics simulations: a hybrid multiphase model for star formation," *MNRAS*, vol. 339, no. 2, pp. 289–311, Feb. 2003.

[82] R. J. J. Grand et al., "The dual origin of the Galactic thick disc and halo from the gas-rich Gaia-Enceladus Sausage merger," *MNRAS*, vol. 497, no. 2, pp. 1603–1618, Sep. 2020.

[83] A. Helmi and P. T. de Zeeuw, "Mapping the substructure in the Galactic halo with the next generation of astrometric satellites," *MNRAS*, vol. 319, no. 3, pp. 657–665, Dec. 2000.

[84] A. Knebe et al., "Mapping substructures in dark matter haloes," *MNRAS*, vol. 357, no. 1, pp. L35–L39, Feb. 2005.

[85] F. A. Gómez et al., "On the identification of merger debris in the Gaia era," *MNRAS*, vol. 408, no. 2, pp. 935–946, Oct. 2010.

[86] G. C. Myeong et al., "Evidence for two early accretion events that built the Milky Way stellar halo," *MNRAS*, vol. 488, no. 1, pp. 1235–1247, Sep. 2019.

[87] ——, "The Sausage Globular Clusters," *ApJ*, vol. 863, no. 2, p. L28, Aug. 2018.

[88] S. R. Majewski et al., "Exploring Halo Substructure with Giant Stars: Substructure in the Local Halo as Seen in the Grid Giant Star Survey Including Extended Tidal Debris from ωCentauri," *ApJ*, vol. 747, no. 2, p. L37, Mar. 2012.

[89] D. Katz et al., "Gaia Data Release 3 Properties and validation of the radial velocities," *arXiv e-prints*, p. arXiv:2206.05902, Jun. 2022.

[90] I. Jean-Baptiste et al., "On the kinematic detection of accreted streams in the Gaia era: a cautionary tale," *A&A*, vol. 604, p. A106, Aug. 2017.

[91] G. Pagnini et al., "The distribution of globular clusters in kinematic spaces does not trace the accretion history of the host galaxy," *arXiv e-prints*, p. arXiv:2210.04245, Oct. 2022.

[92] S. Khoperskov et al., "The stellar halo in Local Group Hestia simulations II. The accreted component," *arXiv e-prints*, p. arXiv:2206.04522, Jun. 2022.

[93] V. Belokurov et al., "Energy wrinkles and phase-space folds of the last major merger," *MNRAS*, vol. 518, no. 4, pp. 6200–6215, Feb. 2023.

[94] V. Belokurov and A. Kravtsov, "From dawn till disc: Milky Way's turbulent youth revealed by the APOGEE+Gaia data," *MNRAS*, vol. 514, no. 1, pp. 689–714, Jul. 2022.

[95] C. Conroy et al., "Birth of the Galactic Disk Revealed by the H3 Survey," *arXiv e-prints*, p. arXiv:2204.02989, Apr. 2022.

[96] H.-W. Rix et al., "The Poor Old Heart of the Milky Way," *ApJ*, vol. 941, no. 1, p. 45, Dec. 2022.

[97] M. Haywood et al., "The age structure of stellar populations in the solar vicinity. Clues of a two-phase formation history of the Milky Way disk," *A&A*, vol. 560, p. A109, Dec. 2013.

[98] M. R. Hayden et al., "Chemical Cartography with APOGEE: Metallicity Distribution Functions and the Chemical Structure of the Milky Way Disk," *ApJ*, vol. 808, no. 2, p. 132, Aug. 2015.

[99] V. Grisoni et al., "The AMBRE project: chemical evolution models for the Milky Way thick and thin discs," *MNRAS*, vol. 472, no. 3, pp. 3637–3647, Dec. 2017.

[100] F. Renaud et al., "Starbursts triggered by intergalactic tides andinterstellar compressive turbulence." *MNRAS*, vol. 442, pp. L33–L37, Jul. 2014.

[101] S. Bustamante et al., "Merger-induced metallicity dilution in cosmological galaxy formation simulations," *MNRAS*, vol. 479, no. 3, pp. 3381–3392, Sep. 2018.

[102] A. Di Cintio et al., "Pericentric passage-driven star formation in satellite galaxies and their hosts: CLUES from local group simulations," *MNRAS*, vol. 506, no. 1, pp. 531–545, Sep. 2021.

Appendix A

Literature Review and Interim Report
width=!,height=!,pages=-